

## FYCO1 and autophagy control the integrity of the haploid male germ cell-specific RNP granules

Matteo Da Ros<sup>a,b,†</sup>, Tiina Lehtiniemi<sup>a,†</sup>, Opeyemi Olotu<sup>a</sup>, Daniel Fischer<sup>c</sup>, Fu-Ping Zhang<sup>a,d</sup>, Helena Vihinen<sup>e</sup>, Eija Jokitalo<sup>e</sup>, Anu Sironen<sup>c</sup>, Jorma Toppari<sup>a,f</sup>, and Noora Kotaja<sup>a</sup>

<sup>a</sup>Institute of Biomedicine, Department of Physiology, University of Turku, Turku, Finland; <sup>b</sup>Department of Cellular and Molecular Biology, Faculty of Medicine, University of Ottawa, Ottawa, ON, Canada; <sup>c</sup>Natural Resources Institute Finland (Luke), Green Technology, Jokioinen, Finland; <sup>d</sup>Turku Center for Disease Modeling, University of Turku, Turku, Finland; <sup>e</sup>Electron Microscopy Unit, Institute of Biotechnology, University of Helsinki, Helsinki, Finland; <sup>f</sup>Department of Pediatrics, University of Turku and Turku University Hospital, Turku, Finland

### ABSTRACT

Ribonucleoprotein (RNP) granules play a major role in compartmentalizing cytoplasmic RNA regulation. Haploid round spermatids that have exceptionally diverse transcriptomes are characterized by a unique germ cell-specific RNP granule, the chromatoid body (CB). The CB shares many characteristics with somatic RNP granules but also has germline-specific features. The CB appears to be a central structure in PIWI-interacting RNA (piRNA)-targeted RNA regulation. Here, we identified a novel CB component, FYCO1, which is involved in the intracellular transport of autophagic vesicles in somatic cells. We demonstrated that the CB is associated with autophagic activity. Induction of autophagy leads to the recruitment of lysosomal vesicles onto the CB in a FYCO1-dependent manner as demonstrated by the analysis of a germ cell-specific *Fyco1* conditional knockout mouse model. Furthermore, in the absence of FYCO1, the integrity of the CB was affected and the CB was fragmented. Our results suggest that RNP granule homeostasis is regulated by FYCO1-mediated autophagy.

### ARTICLE HISTORY

Received 26 January 2016  
Revised 25 October 2016  
Accepted 10 November 2016

### KEYWORDS

autophagy; chromatoid body; FYCO1; germ cell; knockout; lysosome; posttranscriptional; RNP granule; spermatogenesis; vesicle

### Introduction

The genome of meiotic and postmeiotic male germ cells is expressed actively and broadly, which results in the production of a diverse transcriptome that has to be accurately regulated.<sup>1–3</sup> These cells are faced with the responsibility of determining which transcripts should be eliminated and which ones directed for translation or other functions. Furthermore, due to the cessation of transcription in condensing elongating spermatids, long-term mRNA storage is required to supply necessary mRNAs for these transcriptionally inactive cells. To support the multifaceted posttranscriptional control, male germ cells express a high number of RNA-binding proteins, many of which are essential for normal spermatogenesis.<sup>4,5</sup>

Germline cells are characterized by specific cytoplasmic ribonucleoprotein (RNP) granules, or germ granules, that compartmentalize RNA regulatory pathways.<sup>6,7</sup> Different types of germ granules exist in the cytoplasm of given cell types during postnatal spermatogenesis; the most prominent of which are the intermitochondrial cement between the mitochondrial clusters in pachytene spermatocytes and the chromatoid body (CB) in haploid male germ cells.<sup>7</sup> Germ granules consist of both RNA and protein elements, many of which are shared between

different germ granules. For example, Tudor domain-containing proteins, PIWI (P-element-induced *wimpy* testis) proteins and the RNA helicase DDX4/MVH/VASA (DEAD [Asp-Glu-Ala-Asp] box polypeptide 4) are consistently found in all germ granules.

The CB is an unusually large germ granule, about 1  $\mu\text{m}$  in diameter, that starts forming in the cytoplasm of late pachytene spermatocytes. It is condensed to its final form right after meiosis and stays as a distinct cytoplasmic feature throughout the differentiation of round spermatids.<sup>7,8</sup> At the onset of nuclear elongation of spermatids, the CB diminishes in size and forms a ring around the base of the flagellum that takes part in organizing the mitochondrial sheath of the midpiece.<sup>9</sup> Leftover material from the CB is finally discarded with the rest of the cytoplasm in the residual body. In elongating spermatids, the late CB is suggested to change its function, and this transformation is accompanied by the disappearance of typical CB components such as DDX4 and PIWI proteins and the appearance of testis-specific kinases TSSK1 and TSSK2 and their substrate TSRS (testis specific serine kinase substrate).<sup>10</sup>

Successful isolation of CBs from mouse testes has enabled extensive characterization of their molecular composition.<sup>11–13</sup> The

**CONTACT** Noora Kotaja  [noora.kotaja@utu.fi](mailto:noora.kotaja@utu.fi)  Institute of Biomedicine, Department of Physiology University of Turku Kiinamylynkatu 10, 20520 Turku, Finland.

Color versions of one or more of the figures in the article can be found online at [www.tandfonline.com/kaup](http://www.tandfonline.com/kaup).

<sup>†</sup>These authors contributed equally to this work.

 Supplemental data for this article can be accessed on the [publisher's website](#).

© 2017 Matteo Da Ros, Tiina Lehtiniemi, Opeyemi Olotu, Daniel Fischer, Fu-Ping Zhang, Helena Vihinen, Eija Jokitalo, Anu Sironen, Jorma Toppari, and Noora Kotaja. Published with license by Taylor & Francis.

This is an Open Access article distributed under the terms of the Creative Commons Attribution-Non-Commercial License (<http://creativecommons.org/licenses/by-nc/3.0/>), which permits unrestricted non-commercial use, distribution, and reproduction in any medium, provided the original work is properly cited. The moral rights of the named author(s) have been asserted.

CB contains several types of RNAs, including mRNAs, long non-coding RNAs, intergenic transcripts and PIWI-interacting RNAs (piRNAs), as well as a wide variety of RNA-binding proteins.<sup>12</sup> The piRNA pathway is particularly prominent in the CB. The functions of piRNAs are diverse. In prospermatogonia, they play an important role in genome defense by silencing transposon expression<sup>14-17</sup> Postnatal pachytene piRNAs also direct meiotic and postmeiotic mRNAs and long noncoding RNAs for degradation.<sup>18-21</sup> Pachytene piRNAs and PIWI proteins accumulate in the CB, and the current hypothesis is that RNA is targeted to the CB for piRNA-mediated degradation.

The CB is a dynamic structure that actively moves in the cytoplasm of round spermatids in a microtubule-dependent manner.<sup>22</sup> It makes frequent contacts with the nuclear envelope and continuously sends and receives small particles.<sup>23,24</sup> The CB is a nonmembrane bound organelle, but interestingly, it closely communicates with the cellular endomembrane system. It makes frequent contacts with the Golgi complex<sup>25</sup> and it is always associated with multivesicular bodies and small vesicular structures that are often found embedded in the CB pockets.<sup>26</sup>

Recent reports have demonstrated the involvement of autophagy in the assembly and clearance of stress granules that are stress-responsive somatic RNP granules.<sup>27-29</sup> In autophagy, part of the cytosol, including proteins or organelles, is sequestered into a double-membrane structure called a phagophore, which then closes upon itself to form an autophagosome. Autophagosomes subsequently fuse with late endosomes or directly with lysosomes, which leads to the degradation of the cargo by lysosomal proteases.<sup>30</sup> FYCO1 (FYVE and coiled-coil domain containing 1) is a phosphatidylinositol 3-phosphate-binding protein that is involved in the plus end-directed transport of autophagosomes along microtubules.<sup>31</sup> FYCO1 interacts with MAP1LC3/LC3 (microtubule-associated protein 1 light chain 3, LC3 hereafter) proteins<sup>31-33</sup> that are lipidated to be anchored on both sides of the phagophore membrane, where they act in recruitment of cargo and other autophagic proteins to phagophores, as well as in facilitation of phagophore expansion.<sup>34</sup> FYCO1 has also been implicated in the maturation of early phagosomes into late LAMP1 (lysosomal-associated membrane protein 1)-positive phagosomes,<sup>35</sup> in the formation of tubular lysosomes in macrophage cell line upon lipopolysaccharide treatment<sup>36</sup> and in the microtubule-dependent transport of late endosomes via endoplasmic reticulum-endosome contact sites to produce cell protrusions and neurite outgrowth.<sup>37</sup>

The intriguing connection between the nonmembrane-bound CB and cytoplasmic vesicles prompted us to investigate the role of autophagy in the CB function. In this study, we aimed to clarify the nature of the CB-associated vesicles and identify key factors mediating the communication between the CB and the autophagosome/lysosome system.

## Results

### *FYCO1 is a novel CB component*

We took advantage of the recently published CB proteome to explore novel players in CB function. We found that FYCO1 was consistently coprecipitated with the CB<sup>12</sup> (Fig. 1A). FYCO1 was shown to be a ubiquitous protein expressed in all studied tissues, with a relatively high expression level in the testes (Fig. 1B). Both

*Fyco1* mRNA and FYCO1 protein expression increased toward the later time points during the first wave of spermatogenesis (Fig. 1C, D), indicating an increased expression in meiotic and especially postmeiotic cells in comparison to spermatogonia. Immunofluorescence analysis of adult (10 wk) testis sections confirmed that the FYCO1 protein was readily detected in late pachytene spermatocytes, round spermatids and elongated spermatids (Fig. 1E). FYCO1 localized in the cytoplasm, and the signal was concentrated in distinctive granules (Fig. 1E).

Costaining of FYCO1 with the CB markers DDX4, PIWIL1/MIWI (piwi-like RNA-mediated gene silencing 1) and DDX25 (DEAD [Asp-Glu-Ala-Asp] box polypeptide 25) validated that the FYCO1-positive granules in round spermatids represent CBs (Fig. 2A). Colocalization with DDX4 and DDX25 was detected already in the smaller cytoplasmic granules in late pachytene and diplotene spermatocytes that correspond to the CB precursors (Fig. 2B). Interestingly, costaining with TSKS demonstrated that in elongating spermatids, the FYCO1 signal remained in so-called late CBs that are devoid of round spermatid CB markers (Fig. 2A). These results revealed the association between FYCO1 and the CB throughout the existence of this structure, from the formation of CB precursor granules to the late CB stage in elongating spermatids.

Closer examination of the FYCO1 localization in round spermatids demonstrated that the FYCO1 signal did not completely overlap with the DDX4 or PIWIL1 signals. In contrast, FYCO1 appeared to localize in the peripheral region of the CB (Fig. 2C, upper row). Some FYCO1-positive small granules were also observed outside the main CB structure (Fig. 2C, bottom row). To better visualize the localization of FYCO1 in relation to the CB, we created a 3-dimensional model from confocal microscopy z stacks of round spermatids immunostained for FYCO1 and PIWIL2/MILI (piwi-like RNA-mediated gene silencing 2), yet another CB marker (Fig. 2D). Confocal imaging revealed partial overlap of the FYCO1 signal with the PIWIL2 signal at the periphery of the CB. However, the FYCO1 signal also extended outside the PIWIL2-positive CB matrix (Fig. 2D, left panel). Size- and location-wise FYCO1-positive areas matched with the CB-associated vesicles as visualized by electron microscopy (EM; see Fig. 6 for an example). 3D imaging revealed the spreading of the FYCO1 signal at a specific surface of the CB (Fig. 2D, middle and right panels).

To further elucidate the possible membrane association of FYCO1, we performed a tubule culture experiment by incubating stage-specific (II-V) pieces of seminiferous tubules in the absence or presence of wortmannin, a well-characterized inhibitor of phosphatidylinositol 3-kinase.<sup>38</sup> Phosphatidylinositol 3-kinase produces a pool of phosphatidylinositol 3-phosphate that is important for autophagosome formation and maturation.<sup>39-41</sup> FYCO1 has been shown to bind phosphatidylinositol 3-phosphate via its FYVE domain.<sup>31</sup> Interestingly, wortmannin treatment affected the appearance of the CB as detected by anti-DDX25 immunostaining. DDX25-positive CB appeared to form distinct domains, and FYCO1 signal was detected only in a specific CB domain while the other parts of the CB were FYCO1-negative (Fig. 3A to C).

### *FYCO1 interaction partners*

To gain more insight into the role of FYCO1 in the CB function, we identified FYCO1-interacting proteins by

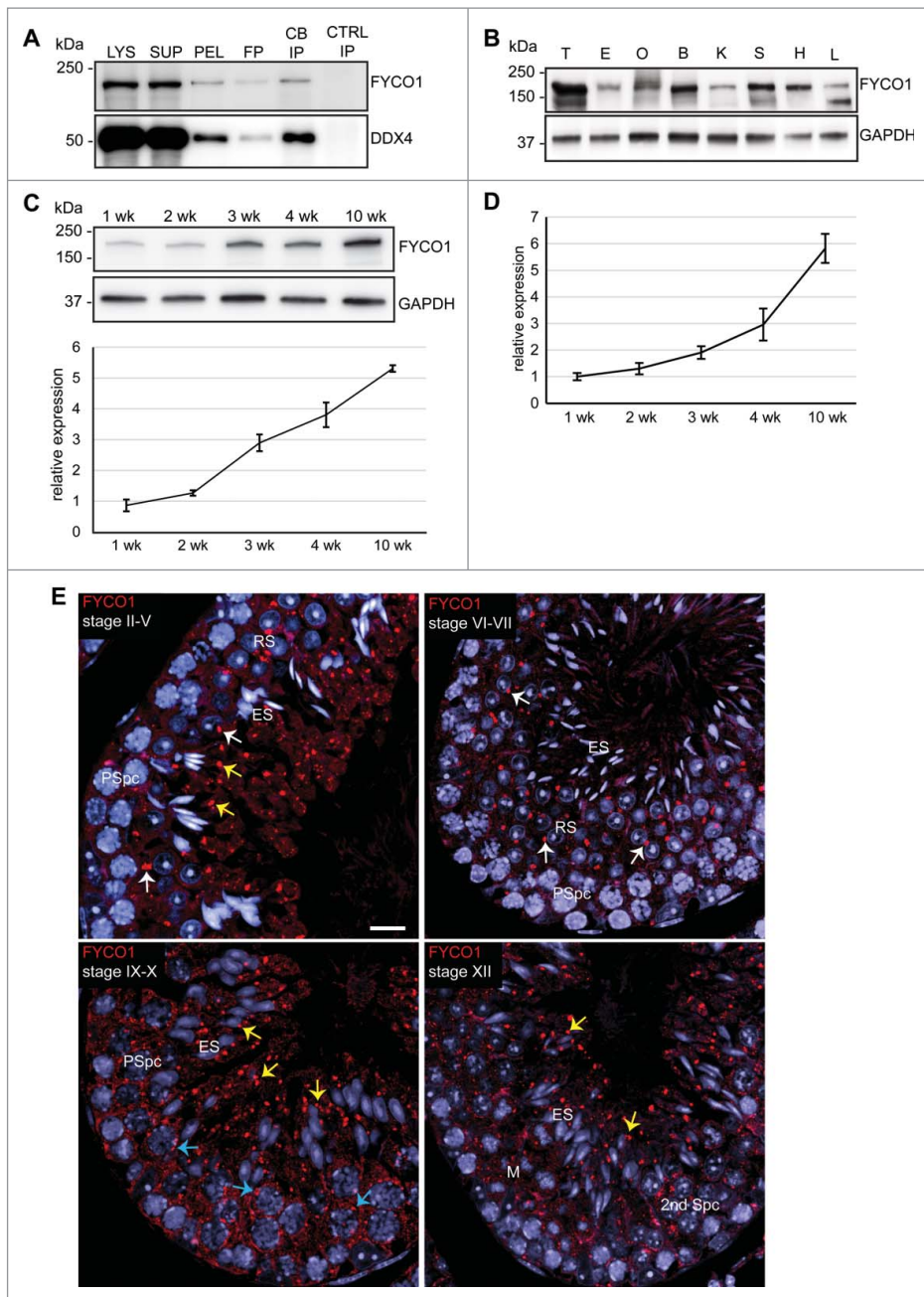


**Figure 1.** Expression of a novel CB component FYCO1 during spermatogenesis. (A) FYCO1 coprecipitates with CBs. CB isolation was performed from cross-linked testicular lysate using anti-DDX4 antibody. FYCO1 was detected in the CB fraction (CB IP) but not in the negative control immunoprecipitated with rabbit IgG (CTRL IP). LYS, testicular cell lysate; SUP, CB-free supernatant fraction after low-speed centrifugation; PEL, CB-containing pellet fraction after low-speed centrifugation; FP, filtered pellet fraction. Immunoblotting with anti-DDX4 confirmed the successful CB isolation. (B) Immunoblotting of tissue lysates using anti-FYCO1 antibody. T, testis; E, epididymis; O, ovary; B, brain; K, kidney; S, spleen; H, heart; L, liver. GAPDH antibody was used as a loading control. (C) Expression of FYCO1 during the first wave of spermatogenesis. Testis samples were collected from juvenile mice at different time points (1 wk, 2 wk, 3 wk, 4 wk, 10 wk/adult). In 1-wk-old testes, spermatogonia exist together with somatic cells. At 2 wk of age, pachytene spermatocytes have appeared; at 3 wk, round spermatids are present; and at 4 wk, spermatid elongation has begun. Anti-GAPDH was used for normalization. Error bars represent standard deviations. (D) Expression of *Fyco1* mRNA during first wave of spermatogenesis as detected by RT-qPCR. Error bars represent s.e.m. of 3 biological replicates. (E) Immunofluorescence analysis of the PFA-fixed paraffin-embedded testis samples (10 wk old) using anti-FYCO1 antibody (red). FYCO1 has granular cytoplasmic staining in round spermatids (white arrows, stages II-V and VI-VII), late pachytene spermatocytes (blue arrows, stage IX-X) and step 9 to 14 elongating spermatids (yellow arrows, stages IX-X, XII and II-V). No FYCO1 signal was detected in step 15 to 16 elongating spermatids at stage VI-VIII. Nuclei were stained with DAPI (blue). PSpc, pachytene spermatocyte; RS, round spermatid; ES, elongating spermatid; M, meiotic metaphase; 2nd Spc, secondary spermatocyte. Scale bar: 10  $\mu$ m.

immunoprecipitating FYCO1 from testis cell lysate and subsequent mass spectrometric analysis. In contrast to the CB isolation protocol, anti-FYCO1 immunoprecipitation was performed without cross-linking, therefore enabling us to concentrate on proteins that form close complexes with FYCO1. Mass spectrometry analysis identified several interaction

partners (Table S1). Some FYCO1-interacting proteins represented CB components, including DDX4, PIWIL2 and TDRD proteins, which reflects the strong association between FYCO1 and the CB. We validated the interaction of FYCO1 with PIWIL2 and another CB protein EIF4A3 (eukaryotic translation initiation factor 4A3), as well as 2 non-CB-associated

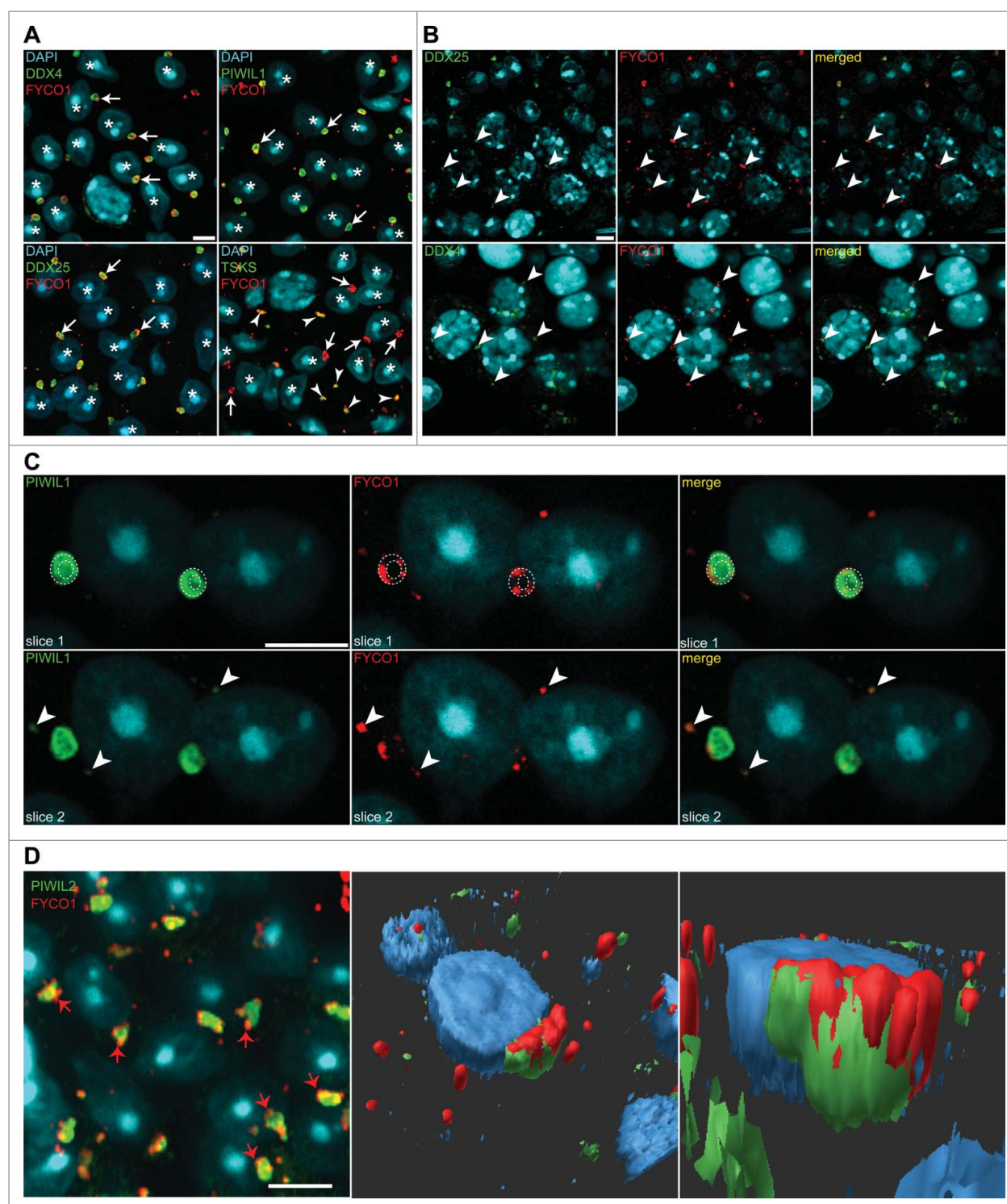


**Figure 2.** FYCO1 localizes to the CBs. (A) Coimmunostaining of FYCO1 (red) with different CB markers DDX4, DDX25 and PIWIL1 (green) in round spermatids. FYCO1 signal is strongly associated with CBs (arrows), which are detected in close contact with round spermatid nuclei (asterisks). Costaining of FYCO1 with TSKS (green) showed the localization of FYCO1 in TSKS-positive late CBs in elongating spermatids (arrowheads) in addition to the localization of the CBs in round spermatids that are negative for TSKS (arrows). Nuclei were stained with DAPI (blue). (B) FYCO1 colocalizes with CB markers DDX25 and DDX4 already in cytoplasmic granules of late pachytene spermatocytes (arrowheads). (C) The FYCO1 signal is not concentrated on the core CB matrix but in the peripheral areas of the CB, dashed circles are drawn as a reference. Some non-CB-associated small FYCO1 granules can be detected in the cytoplasm or round spermatids (arrowheads). Upper and lower images in (C) represent different slices of a stack obtained by laser-scanning confocal microscopy of the same sample. Scale bars: 5  $\mu$ m. (D) 3D modeling of the FYCO1 (red) localization in relation to the PIWIL2-positive CB (green). In the confocal image, red arrows point to the FYCO1-positive areas at the periphery of the CB that are not overlapping with the PIWIL2 signal. Scale bar: 5  $\mu$ m. Middle and right panels show 2 different views of the 3D modeling of the confocal z stack immunostained with anti-PIWIL2 (green) and anti-FYCO1 (red) antibodies.

proteins RUVBL1 (RuvB-like protein 1) and RUVBL2 (RuvB-like protein 2) by anti-FYCO1 immunoprecipitation followed by western blotting with specific antibodies (Fig. 4A).

Interestingly, PIWIL1 was not identified in the mass spectrometric analysis, nor was it detected in the anti-FYCO1 immunoprecipitation by western blotting (Fig. 4A). The analysis of

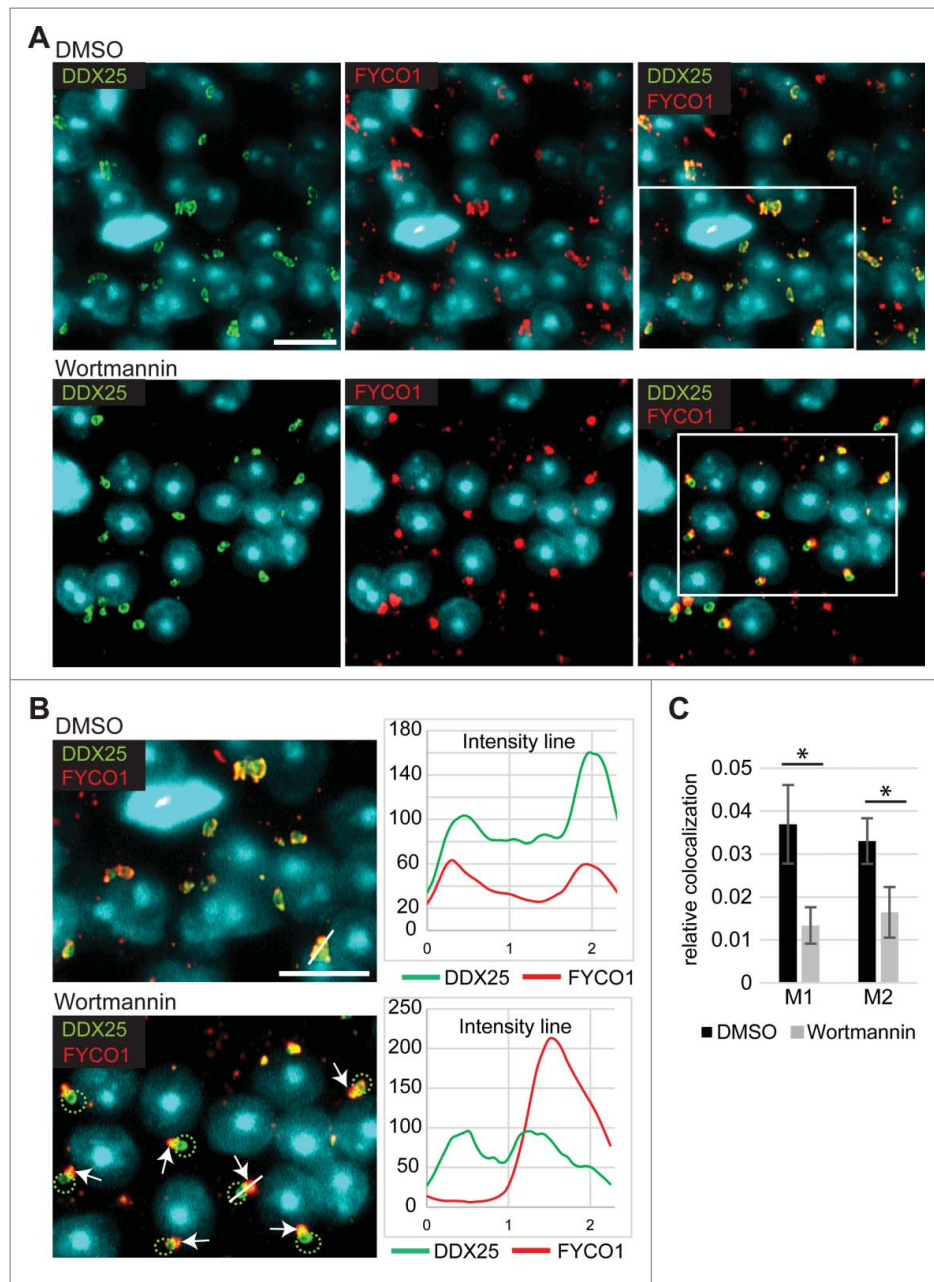


**Figure 3.** Inhibition of phosphoinositide 3-kinases affects the CB localization of FYCO1. (A) Stage-specific pieces of seminiferous tubules (II-V) from wildtype mice were incubated with DMSO or wortmannin for 6 h. After cultures, squash preparations were made and immunostained with anti-DDX25 (green) and anti-FYCO1 (red) antibodies. Nuclei were stained with DAPI. (B) A closer look at the DMSO- and wortmannin-treated tubules immunostained with anti-DDX25 and anti-FYCO1 antibodies. Arrows indicate the CB domain with accumulated FYCO1 signal after wortmannin treatment, and DDX25-positive CB domains devoid of FYCO1 signal are circled with dashed green line. Scale bars: 10  $\mu$ m. Intensity line graphs show fluorescence intensity of FYCO1 (red) and DDX25 (green) along the white lines drawn on the images. (C) Quantification of the colocalization of FYCO1 and DDX25 after wortmannin treatment using Manders coefficients. M1 represents the relative amount of red pixels (FYCO1) colocalizing with green pixels (DDX25), while M2 represents the relative amount of green pixels colocalizing with red pixels. Error bars represent standard deviations. Significant reduction of colocalization was detected in both groups ( $*P$  value  $\leq 0.05$ ).

FYCO1 localization in *piwill* and *tdrd6* (tudor domain containing 6) knockout germ cells demonstrated that at least these 2 major CB components were not required for the CB-localization of FYCO1; even though CB morphology is greatly affected in the absence of PIWIL1 or TDRD6,<sup>42-44</sup> FYCO1 still localized in the CB area in *piwill* and *tdrd6* knockout spermatids (Fig. S1).

GO (gene ontology) term analysis demonstrated that the FYCO1-interacting proteins were enriched under the GO terms connected to microtubule- and vesicle-related processes (Table S1). The most significant GO terms included e.g.

“microtubule-based process” and “macromolecule localization,” but also male germ cell differentiation-related terms such as “spermatogenesis” (Fig. 4B). Closer examination of the proteins revealed that a number of kinesin motor proteins such as KIF5C, KIF3A and KIF3B that are involved in microtubule-mediated transport were identified as FYCO1-interacting proteins (Table S1). These results suggest that the somatic function of FYCO1 in microtubule-mediated vesicle transport<sup>31,37</sup> is conserved in male germ cells. Altogether 20 of the FYCO1-interacting proteins were CB proteins, while 46 and 38 of them were associated with the GO terms “vesicle” and “microtubule-

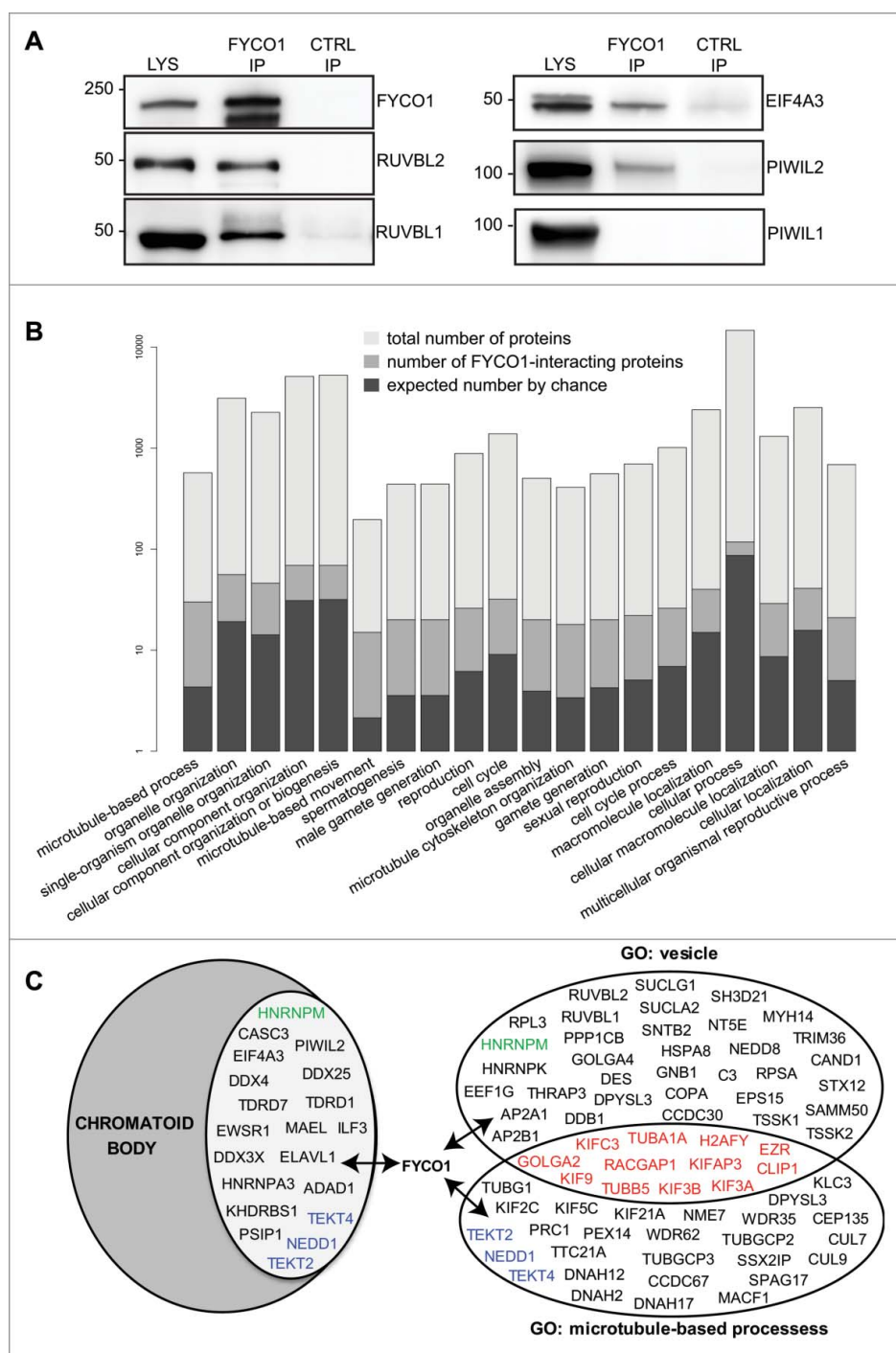


**Figure 4.** FYCO1 interacts with CB components and proteins involved in vesicle trafficking and microtubule-mediated transport. (A) Coimmunoprecipitation using anti-FYCO1 antibody followed by western blotting with anti-FYCO1, anti-RUVBL1, anti-RUVBL2, anti-EIF4A3, anti-PIWIL2 and anti-PIWIL1 antibodies. Immunoprecipitation using rabbit IgG (CTRL IP) was used as a negative control. LYS, protein lysate before immunoprecipitation. (B) Twenty most significant GO terms for FYCO1-interacting proteins. The graph shows the total number of proteins listed under each GO term (light gray), the number of FYCO1-interacting proteins found in each GO term (dark gray), and the number of proteins expected to be found by chance (black). For better comparability, the total numbers are log transformed. (C) FYCO1-interacting proteins contained 20 CB proteins, 46 proteins under the GO term “vesicle” and 38 proteins under the GO term “microtubule-based process.” 12 proteins that are listed under both GO terms are shown in red.

based process,” respectively (Fig. 4C). Interestingly, FYCO1-interacting proteins also included several proteins involved in the ubiquitin pathway, such as the E3 ubiquitin protein ligase HERC2 (HECT and RLD domain containing E3 ubiquitin protein ligase 2), TRIM36 (tripartite motif-containing 36) and UBR4 (ubiquitin protein ligase E3 component n-recognin 4) as well as several CULLIN proteins (CUL9, CUL7, CUL4A),

which are core components of the ubiquitin-protein ligase complexes (Table S1).

#### **CB is disintegrated in *Fyco1* knockout round spermatids**

To elucidate the function of FYCO1 during spermatogenesis *in vivo*, we generated a conditional male germ cell-specific

*Fyco1* knockout mouse model by crossing floxed *Fyco1* mice with mice carrying *Neurog3* promoter-driven Cre expression (*Fyco1<sup>fx/fx</sup>;Neurog3 Cre<sup>+</sup>*). These mice are called *Fyco1* conditional knockout (cKO) in this study. As controls, we used mice carrying a floxed *Fyco1* gene without Cre

expression (*Fyco1<sup>fx/fx</sup>;Neurog3 Cre<sup>-</sup>*). The decreased expression of FYCO1 in the cKO testes was demonstrated by western blot analysis (Fig. 5A). Immunofluorescence analysis validated the absence of FYCO1 in *Fyco1* cKO germ cells (Fig. 5B).

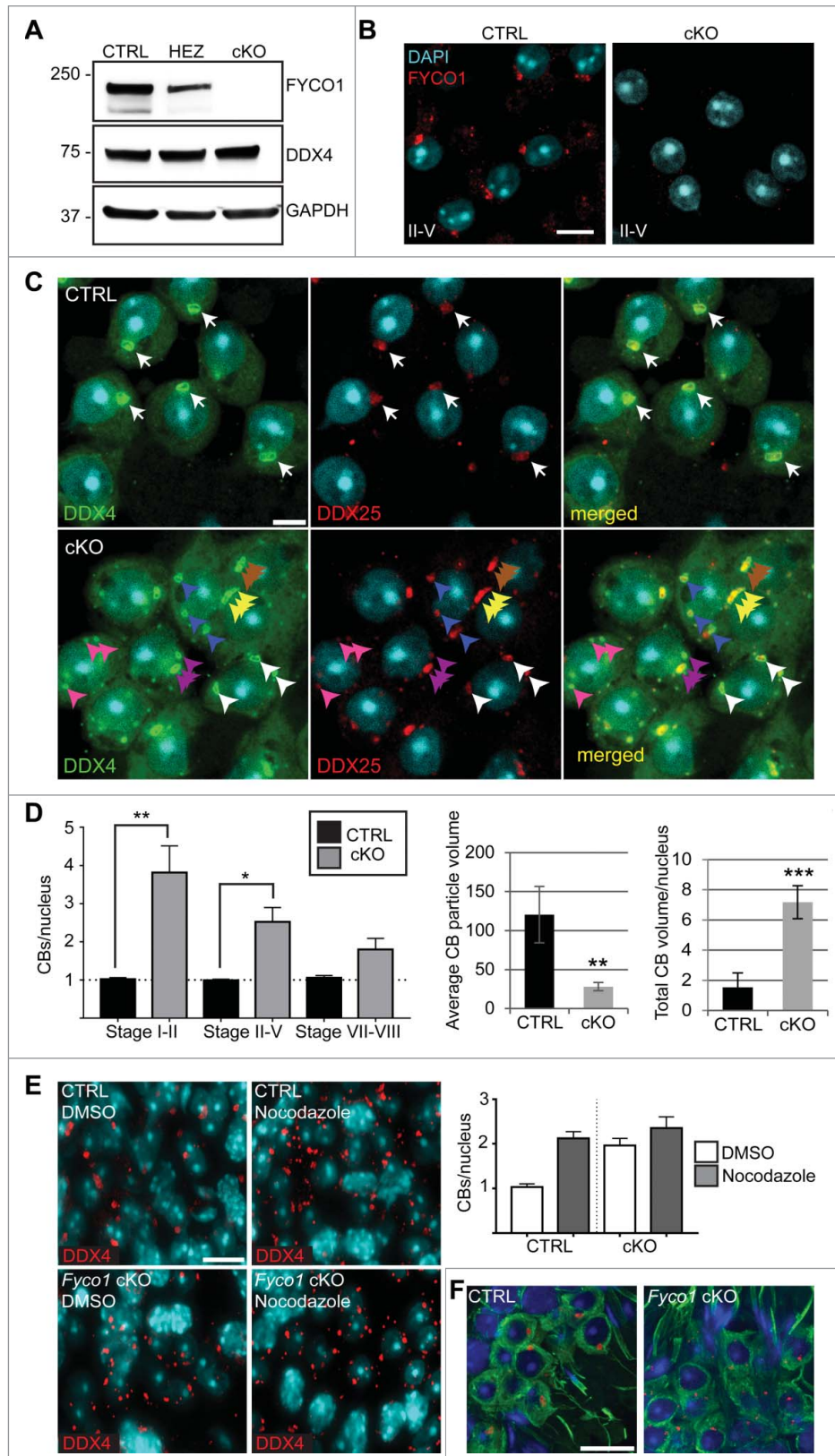


Figure 5. (For figure legend, see page 309).

Examination of CB in *Fyco1* cKO round spermatids revealed that the CBs were clearly affected as detected by immunofluorescence staining using CB markers DDX4 and DDX25; CBs were smaller in size and several CBs were found in the cytoplasm of round spermatids compared with only one prominent structure in control cells (Fig. 5C). Quantification of the CB fragmentation revealed increased number of DDX4-positive granules per nuclei in early (stage I), mid (stage II-V) and late (stage VII-VIII) round spermatids (Fig. 5D). The fragmentation appeared to be more prominent in early steps of round spermatid differentiation. Furthermore, the size of individual DDX4-positive granules was reduced in *Fyco1* cKO round spermatids, but, interestingly, the area occupied by DDX4-positive granules per nuclei was increased, suggesting a defective turnover of the CB material (Fig. 5D).

Similar CB fragmentation was detected after treatment of seminiferous tubules with nocodazole, which inhibits microtubule polymerization (Fig. 5E).<sup>22</sup> However, nocodazole treatment did not further enhance the CB fragmentation caused by *Fyco1* deletion (Fig. 5E). Considering the established function of FYCO1 in microtubule-mediated transport,<sup>31,37</sup> these observations support a model in which FYCO1, by its interaction with the microtubule system, is involved in the correct assembly of the CB. The general organization of microtubule network appeared unaffected in *Fyco1* cKO round spermatids (Fig. 5F).

Interestingly, FYCO1-dependent processes are clearly compensated by other mechanisms in the absence of FYCO1 since testis and epididymis weights in *Fyco1* cKO mice appeared normal and we did not observe any abnormalities in spermatogenesis or in the morphology of epididymal spermatozoa (Figs. S2 and S3). Furthermore, *Fyco1* cKO males produced a comparable number of pups to control males when mated with C57BL/6 females (Fig. S3).

### Transcriptomic profiling of *Fyco1* cKO round spermatids

To find out if the deletion of *Fyco1* affects the CB-mediated regulation of the round spermatid transcriptome, we performed poly-A RNA profiling of *Fyco1* cKO and control round spermatids by deep sequencing. The analysis of differentially expressed (DE) genes revealed that the majority of mRNAs were expressed at comparable levels in cKO and control round spermatids (Table S2). However, 322 genes were found to be significantly misregulated ( $P$  value  $\leq 0.05$ ) in *Fyco1* cKO germ cells. Downregulation of *Bloc1s6* (biogenesis of lysosomal organelles

complex-1, subunit 6, pallidin) and *Spg11* (spastic paraplegia 11), and upregulation of *Rpap3* (RNA polymerase II associated protein 3) mRNAs in *Fyco1* cKO round spermatids were validated by RT-qPCR (Fig. S4A). GO term analysis showed that the genes upregulated in *Fyco1* cKO round spermatids were overrepresented under the GO terms connected to cell response to different stimuli, differentiation/morphogenesis and regulation of biological quality (Table S3).

In addition to mRNAs, the CB accumulates other transcripts such as piRNAs, piRNA precursors and nonannotated intergenic transcripts (termed CB-associated novel transcripts in this study).<sup>12</sup> Mature piRNAs were not sequenced, but SYBR Gold staining of total testis RNA revealed that piRNA were detected at comparable levels in the control and *Fyco1* cKO round spermatids (Fig. S4B). Out of 141 piRNA precursor transcripts detected in our RNA sequencing analysis, 6 were significantly misregulated ( $P$  value  $\leq 0.05$ ) (Table S2). When analyzing CB-associated novel transcripts, we detected 47 significantly misregulated ones in the absence of FYCO1 (Table S2). We also analyzed expressions of transcripts from nonannotated genomic regions predicted by Cufflinks. Out of 19,585 predicted transcripts we obtained 499 DE genes ( $P$  value  $\leq 0.05$ ) (Table S4). Interestingly, the analysis of chromosomal origins of these transcripts revealed a concentration on specific regions of chromosomes 8 and 12 (Fig. S4C). We did not detect any clear differences in the expressions of transposons in *Fyco1* cKO round spermatids (Table S5).

### FYCO1 is required for the association of autophagosomes/autolysosomes with the CB

Close examination of CB-associated vesicles by EM revealed that they often have a double-membrane c-shaped appearance and size varying between 100 to 200 nm (Fig. 6A). Furthermore, these vesicles typically appeared to be cup-shaped in electron tomography imaging (Fig. 6B).<sup>26</sup> Although smaller in size than starvation induced phagophores in cultured cells (300 to 600 nm), these cup-shaped vesicles shared similar features with phagophores, including 2 limiting membranes that appear contrasted, which is typical for forming autophagosomes.<sup>45,46</sup> While the exact nature of these vesicles remains to be characterized, the presence of LC3B-positive vesicles in the CB surroundings suggests that they could be involved in the autophagic pathway (Fig. 6C). In addition to the LC3B-positive vesicles that were interacting with the CB, a larger area of

**Figure 5.** (see previous page) FYCO1 is required for the integrity of the CB. (A) Immunoblotting of adult testicular lysate using anti-FYCO1 antibody validated the dramatically lowered amount of FYCO1 in the germ cell-specific *Fyco1* cKO testes. DDX4 expression levels were unaltered in cKO testes. Anti-GAPDH immunoblotting demonstrated the equal loading of proteins in each lane. CTRL: *Fyco1*<sup>flox/flox</sup>; *Neurog3* Cre<sup>-</sup>, HEZ: *Fyco1*<sup>flox/wt</sup>; *Neurog3* Cre<sup>+</sup>, cKO: *Fyco1*<sup>flox/flox</sup>; *Neurog3* Cre<sup>+</sup>. (B) Immunofluorescence staining using anti-FYCO1 antibody (red) confirmed the absence of FYCO1 expression in the *Fyco1* cKO round spermatids. Nuclei were stained with DAPI. Scale bar: 10  $\mu$ m. (C) The integrity of the CB was examined by immunofluorescence analysis using CB markers DDX4 (green) and DDX25 (red). Nuclei were stained with DAPI. CBs in wild-type samples are indicated with white arrows. Fragmented CBs in cKO tissues are indicated with arrowheads; fragments representing the CB of one cell are marked with arrowheads of the same color. Scale bar: 5  $\mu$ m. (D) The number of CB fragments (DDX4-positive granules) per nucleus at different phases of differentiation (stages I-II, II-V, VII-VIII) was increased in *Fyco1* cKO compare with control round spermatids. The change was significant at stage I-II (\*\* $P$  value  $\leq 0.01$ , 2-tailed  $t$ -test) and stage II-V (\* $P$  value  $\leq 0.05$ , 2-tailed  $t$  test). For each stage, 50 nuclei were counted in each of 3 replicates. For a second graph, DDX25-positive granules were segmented using BioimageXD to calculate the average volume (in voxels) of DDX25-positive CBs (\*\* $P$  value  $\leq 0.01$ , 2-tailed  $t$  test). For a third graph, DDX4-positive granules were segmented and the total volume of DDX4-positive CBs (in voxels) was normalized by the number of nuclei marked by DAPI (\*\*\* $P$  value  $\leq 0.001$ , 2-tailed  $t$  test). Error bars represent standard deviations. (E) Pieces of stage IV-VI seminiferous tubules from control and *Fyco1* cKO mice were cultured for 6 h in the absence (DMSO) or presence of the microtubule disrupting chemical nocodazole. Immunofluorescence staining of the squashed preparations from the cultured seminiferous tubules was performed with anti-DDX4 antibody (red). Scale bar: 10  $\mu$ m. Quantification demonstrates the number of DDX4-positive fragments per nucleus after nocodazole treatment in control and *Fyco1* cKO round spermatids. For each condition, 50 nuclei were counted in each of 3 replicates. (F) PFA-fixed paraffin-embedded testis sections were immunostained with anti-TUBULIN (green) and anti-DDX25 (red). Nuclei were stained with DAPI. Scale bar: 10  $\mu$ m.

accumulated LC3B signal was consistently found in the proximity of the CB (Fig. 6C, bottom panel). This area could correspond to the accumulation of membrane structures found in the electron tomography slices, containing similar cup-shaped structures found in the CB, but also a larger phagore-

resembling structure with electron dense, CB-like material inside the lumen (Fig. S5).

FYCO1 has been reported to be a RAB7- and LC3-interacting protein involved in microtubule-dependent transport of autophagosomes and late endosomes in somatic cells.<sup>31,37</sup> This

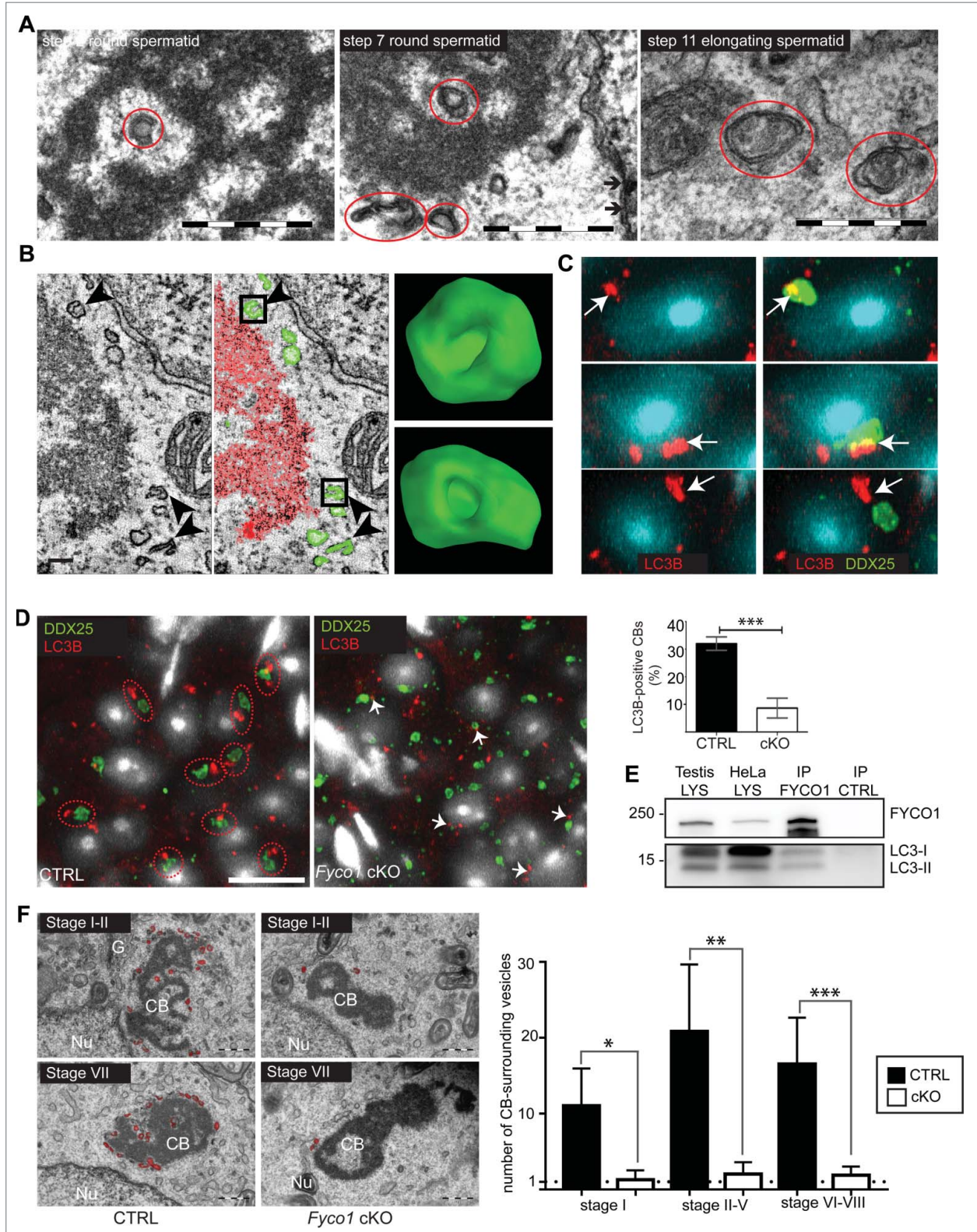


**Figure 6.** (For figure legend, see page 311).

prompted us to explore the possible role of FYCO1 in the communication between the CB and autophagosomes/lysosomes. Coimmunofluorescence analysis of LC3B and the CB marker DDX25 showed that in *Fyco1* cKO round spermatids, the association of CB fragments with LC3B signal was clearly reduced; 32% of the control CBs, but only 9% of cKO CBs, had overlapping LC3B signal (graph in Fig. 6D). Furthermore, LC3B-positive clouds that were consistently detected in the proximity of control CBs were not present in *Fyco1* cKO spermatids (Fig. 6D). In the absence of FYCO1, LC3B vesicles were more evenly distributed in the cytoplasm, and no clear accumulation in the CB region was detected. Anti-FYCO1 immunoprecipitation from testicular vesicle-containing organelle fractions revealed that the somatic LC3B-binding activity of FYCO1<sup>31</sup> was conserved in male germ cells (Fig. 6E). This suggests that FYCO1 is directly involved in the recruitment of LC3B-positive vesicle into the CB. The lack of CB-associated vesicles in the absence of FYCO1 was also confirmed by electron microscopy (Fig. 6F).

### **FYCO1 is required for the recruitment of lysosomal vesicles to the CB upon induction of autophagy**

To study the connection between the CB and autophagy more carefully, we cultured stage-specific (stage II-V) pieces of the seminiferous tubules in the absence and presence of autophagy modulators. We used LAMP1 as a marker to detect lysosomes and autolysosomes. Under control conditions (DMSO only), LAMP1-positive vesicles were detected widely in the cytoplasm of round spermatids (Fig. 7A). The LAMP1 signal was also concentrated in the peripheral areas of the CB, as shown earlier by immunoelectron microscopy.<sup>47</sup> Treatment of cells with rapamycin, which inhibits the Ser/Thr protein kinase MTOR (mechanistic target of rapamycin) and induces autophagy, resulted in the strong accumulation of the LAMP1 signal on the CB (Fig. 7A). Incubation of the tubules with bafilomycin A<sub>1</sub> (Baf), which inhibits the late phase of autophagy by preventing fusion between autophagosomes and lysosomes, resulted in the accumulation of LAMP1-positive vesicles next to the CB (Fig. 7A). In *Fyco1* cKO seminiferous tubules, rapamycin did not induce accumulation of LAMP1-positive vesicles onto the CB. In addition, Baf did not have any effect on the LAMP1 localization pattern in *Fyco1* cKO round spermatids (Fig. 7A). Quantification of colocalization using Manders coefficients showed that both rapamycin and Baf caused an increase in the overlap of LAMP1 and DDX25 signal in control round

spermatids, while they did not enhance the colocalization in *Fyco1* cKO cells (Fig. 7B).

### **FYCO1 regulates the expression level of PIWIL2**

We performed western blot analysis of total testis extracts to study the effects of FYCO1 inactivation on the expression levels of selected proteins. While the levels of other studied proteins were not affected, we revealed that the amount of PIWIL2 was significantly reduced in *Fyco1* cKO testes compare with control testes (Fig. 8A). Interestingly, another PIWI protein PIWIL1 was not significantly affected, correlating with the fact that we did not detect an interaction between FYCO1 and PIWIL1 in coimmunoprecipitation experiments (Fig. 4A). Despite the downregulation of PIWIL2 expression, PIWIL2 was found to be correctly localized in the intermitochondrial cement of pachytene spermatocytes and fragmented CBs in step 1 round spermatids (Fig. 8B). The localization of PIWIL1 was also unaffected in *Fyco1* cKO testes (Fig. 8B).

To study the effects of induced autophagy on PIWIL2 expression, we performed tubule culture experiments by incubating a batch of 30 segments of seminiferous tubules in the absence or presence of rapamycin and Baf. Rapamycin treatment caused significant downregulation of PIWIL2 levels in control tubules, but in contrast, it had no significant effect on PIWIL2 levels in *Fyco1* cKO tubules (Fig. 8C). Baf did not affect PIWIL2 levels under the conditions used for the experiment (6 h incubation at 34°C). These results suggest that FYCO1 is required for the rapamycin-induced downregulation of PIWIL2 in male germ cells.

## **Discussion**

Compartmentalized RNA regulation in the cytoplasmic RNP granules affords a powerful means for accurate control of the cellular transcriptome. The formation, function and homeostasis of RNP granules has to be strictly monitored, and increasing evidence supports the integral role of the vesicular transport system in their regulation.<sup>27-29</sup> The interplay between RNP granules and the endomembrane system is beautifully exemplified by the haploid male germ cell-specific RNP granule, the CB, which is surrounded by small cytoplasmic vesicles and multivesicular bodies and dynamically communicates with the nuclear envelope and the Golgi complex.<sup>7,48</sup> In this study, we revealed that CB-associated vesicles are involved in the autophagy-lysosomal pathway as suggested by the accumulation of LC3B and LAMP1 signal in the CB surroundings. Importantly,

**Figure 6.** (see previous page)The CB associates with vesicles in a FYCO1-dependent manner. (A) In electron microscopy, some of the CB-associated vesicles resemble phagophores (red circles in left and middle panel), although smaller in size than non-CB-associated phagophores (red circles in right panel). Arrows point to the nuclear envelope. Scale bar: 500 nm. (B) Electron tomography visualized the cup-like shape of CB-associated vesicles (arrowheads). Left panel: electron tomography, scale bar: 500 nm, middle panel: segmentation of the CB (red) and small cytoplasmic vesicles (green), right panels: 3D surface reconstruction of 2 representative vesicles. (C) Immunofluorescence analysis of paraffin-embedded testis sections with anti-DDX25 (green) and anti-LC3B (red) antibodies. LC3B-positive structures (arrows) can be found in the CB (upper and middle images) and accumulated in a close proximity of the CB (bottom images). Nuclei were stained with DAPI. (D) Accumulations of the LC3B signal close to the CB in control round spermatids (CTRL) are indicated with red dashed circles. These LC3B-positive clouds were absent in *Fyco1* cKO spermatids, and only small LC3B vesicles were found distributed in the cytoplasm, sometimes making contact with the CB (white arrows). Scale bar: 10 μm. A graph shows the significant reduction (\*\*\*) *P* value ≤ 0.001, 2-tailed *t*-test) in CBs that overlap with LC3B signal in cKO round spermatids. (E) Anti-FYCO1 immunoprecipitation was performed from the round spermatid vesicle-containing fraction. Immunoblotting with anti-LC3B showed a coprecipitation of both LC3-I and LC3-II with FYCO1 (IP FYCO1), but not with rabbit IgG-bound beads (IP CTRL). Testis LYS, input lysate that was used as a starting material for immunoprecipitation. HeLa LYS, lysate from starved HeLa cells. (F) Electron microscopic analysis of control and *Fyco1* cKO CBs. Two different stages of the seminiferous epithelial cycle containing either early- (stage I-II) or late-round spermatids (stage VII) are shown. CB-associated vesicles are painted in red. G, Golgi complex; Nu, nucleus. Scale bar: 500 nm. Quantification of CB-associated vesicle at 3 different developmental stages (stages I, II-V and VI-VIII) revealed a dramatic reduction of vesicles surrounding *Fyco1* cKO CBs. Error bars represent standard deviations. *P* values range from \**P* value ≤ 0.05 to \*\*\**P* value ≤ 0.001 (2-tailed *t* test) analyzed by GraphPad Prism 7.0.

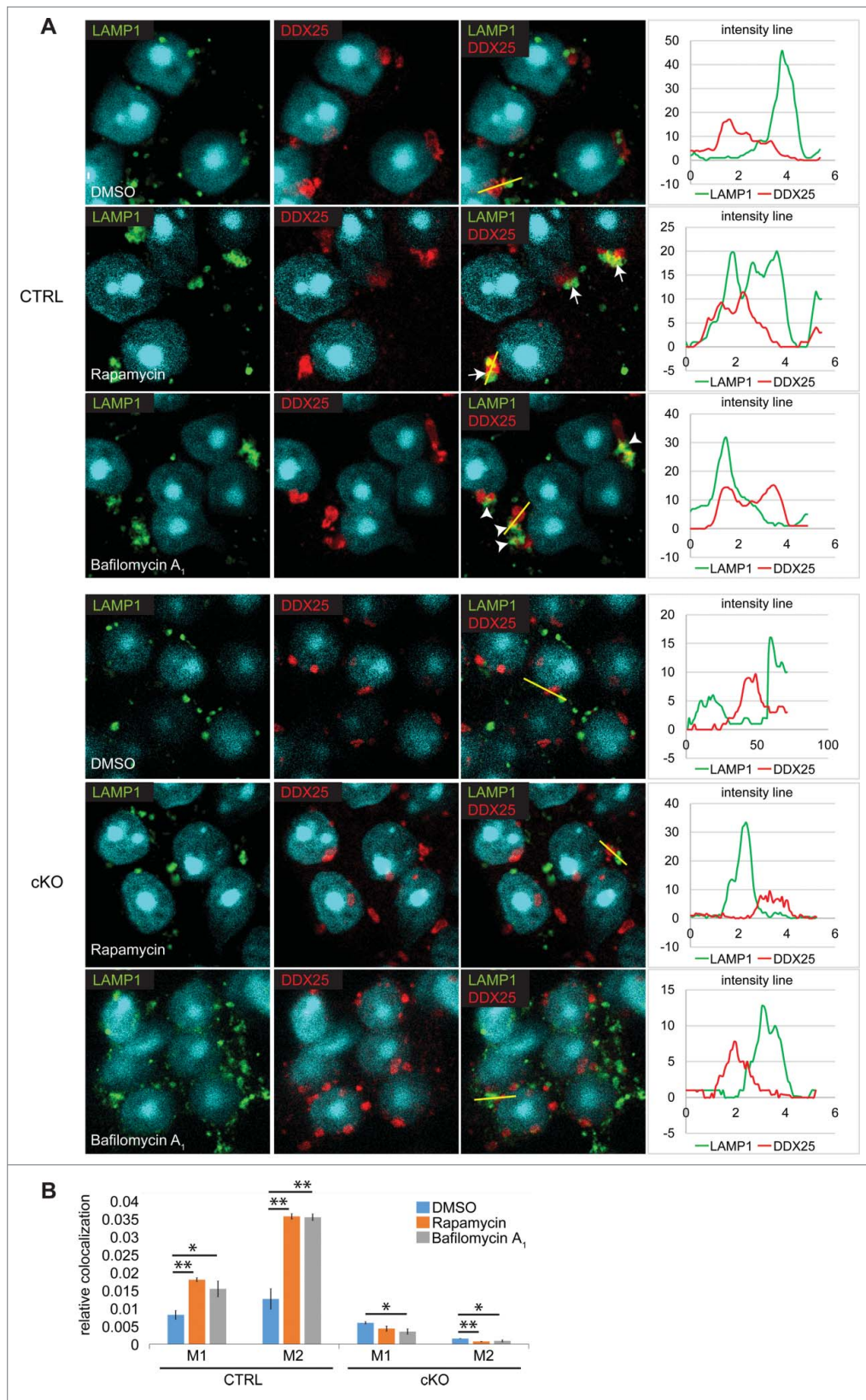


**Figure 7.** Lysosomal vesicles are not recruited to the CB in the absence of FYCO1. (A) Stage-specific (II-V) pieces of the control (CTRL) or *Fyco1* cKO (cKO) seminiferous tubules were cultured in the presence of vehicle (DMSO), rapamycin or Baf. After cultures, squash preparations were made and immunostained with anti-DDX25 (red) and anti-LAMP1 (green) antibodies. Nuclei were stained with DAPI (blue). Arrows point to the LAMP1-signal recruited in the CB area after rapamycin treatment. Accumulations of LAMP1-positive vesicles next to the CB after Baf treatment are indicated by arrowheads. Scale bar: 10  $\mu$ m. Intensity of LAMP1 and DDX25 signal was measured along the yellow lines to reveal the spatial localization of LAMP1-positive vesicles and the CB. (B) Colocalization of LAMP1 with DDX25 in control and cKO testis treated with rapamycin, Baf or the vector (DMSO) was measured using Manders coefficients. Error bars represent standard deviations.

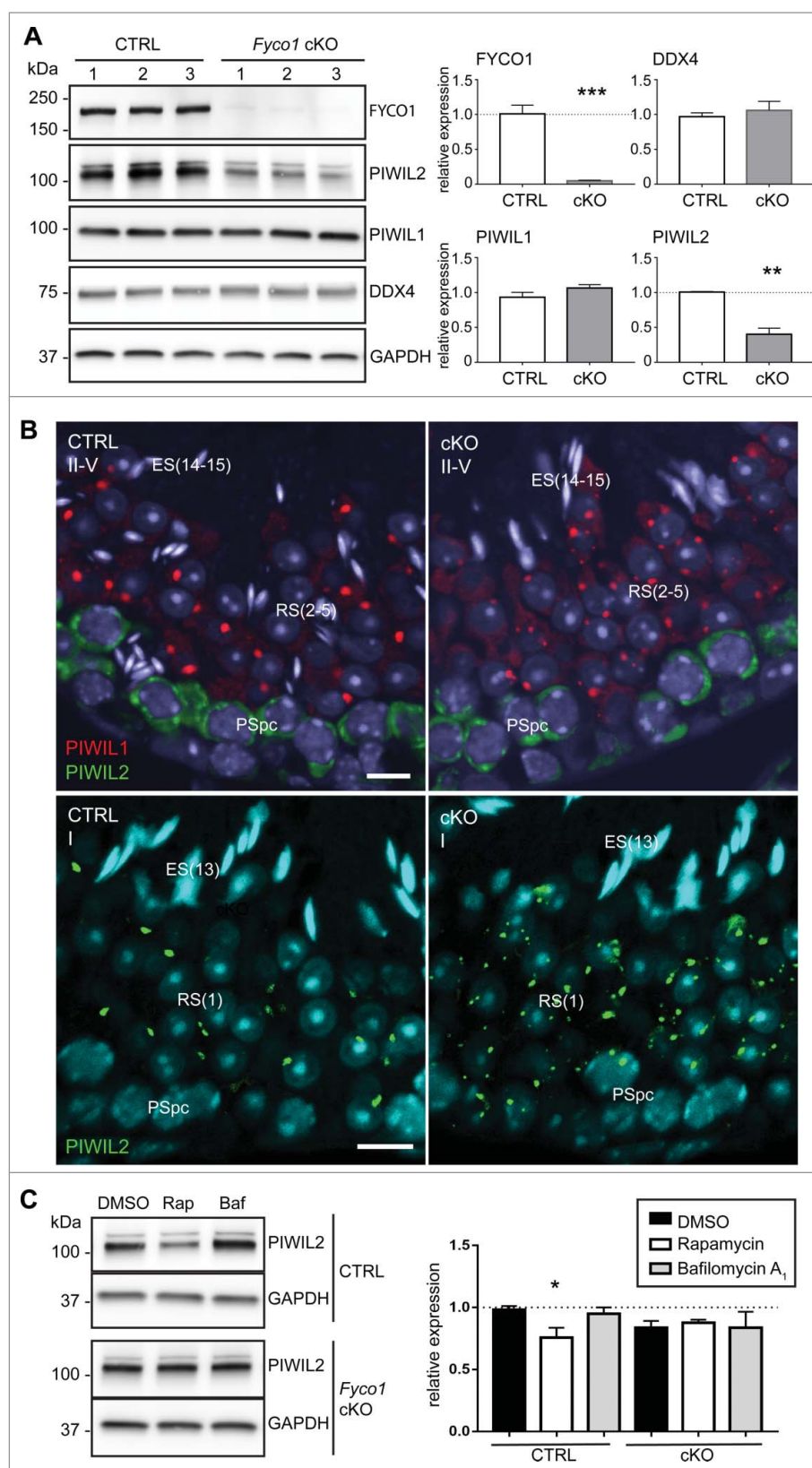


**Figure 8.** PIWIL2 is downregulated in *Fyco1* cKO testes. (A) Western blot images for expression of FYCO1, PIWIL2, PIWIL1, DDX4 and GAPDH in control and *Fyco1* cKO testes (3 biological replicates per genotype). Quantification revealed significantly lowered amount of PIWIL2 in *Fyco1* cKO testes (\*\**P* value  $\leq 0.01$ ; 2-tailed *t* test). The expression levels of PIWIL1 and DDX4 were unaltered. Anti-GAPDH signal was used for the normalization. Error bars represent s.e.m. (B) Immunofluorescence analysis of paraffin-embedded testis sections at stage II-V (PIWIL1: red, PIWIL2: green) and stage I (PIWIL2: green) in control (CTRL) and *Fyco1* cKO (cKO) mice. Nuclei were stained with DAPI. PSpC, pachytene spermatocyte; RS, round spermatid; ES, elongating spermatid. The roman numbers in parentheses after RS or ES represent the step of spermatid differentiation. Scale bar: 10  $\mu$ m. (C) Segments of seminiferous tubules of control and *Fyco1* cKO mice were incubated with DMSO, rapamycin (Rap) or Baf (30 segments/treatment) and PIWIL2 was detected with a specific antibody. The western blotting image represents one of the 3 biological replicates that were used for quantification. Anti-GAPDH signal was used for normalization. The average of 3 biological replicates are shown. Error bars represent s.e.m. \**P* value  $\leq 0.05$ ; 2-tailed *t* test.

we identified an LC3B-interacting protein FYCO1 as a novel CB component that mediates the association of the vesicles with the CB and controls the recruitment of lysosomes onto the CB when autophagy is induced.

The dramatic accumulation of LAMP1-positive lysosomes onto the CB upon induction of autophagy suggests a central role for the CB in the catabolic activity of haploid male germ cells. In somatic cells, lysosome position has been shown to coordinate autophagy via the MTOR pathway. Under nutrient-rich conditions, lysosomes localize in the cell periphery, while during starvation, they are clustered in the perinuclear area in a microtubule-dependent manner, which facilitates fusion of lysosomes with autophagosomes.<sup>49</sup> We suggest that a similar process takes place in haploid male germ cells: the content of the autophagosomes formed in the vicinity of the CB is targeted to degradation by fusion with lysosomes, and the rate of autophagy is increased upon rapamycin treatment by active recruitment of lysosomes to the CB.

The analysis of *Fyco1* cKO round spermatids revealed that FYCO1 functions as a docking platform for LC3 or LAMP1-positive membranes and mediates autophagosome and lysosome recruitment to the CB. Autophagy could provide a potential mechanism for the clearance of CB material and the maintenance of CB homeostasis. Electron dense material is indeed sometimes found inside CB-associated cup-shaped vesicles, and we have also detected larger phagophore-resembling structures with CB material in the lumen in the vicinity of the CB (Fig. S5). Although the total DDX4 level in the testis was not found to be significantly increased in *Fyco1* cKO mice, the total volume of DDX4-positive granules per nuclei as detected by immunofluorescence analysis was increased, suggesting an increase in the CB material. We also revealed that the expression level of one of the PIWI proteins, PIWIL2, was compromised in the absence of FYCO1, and further investigation showed that PIWIL2 was targeted for degradation upon induction of autophagy in a FYCO1-dependent manner. Interestingly, several factors involved in the ubiquitin-proteasome pathway were identified as FYCO1-interacting proteins. Targets of selective autophagy are often ubiquitinated, which enables their recognition by receptor proteins and targeting to the LC3-containing autophagosomes.<sup>50,51</sup> The complex formation between FYCO1 and ubiquitin E3 ligases suggests the involvement of protein ubiquitination in the CB-associated autophagy.

In addition to the digestion of bulk CB material, an intriguing option is that some specific RNA species are eliminated from the CB by FYCO1-mediated autophagy. It has recently been demonstrated that autophagy can protect genomic stability by degrading retrotransposon RNA.<sup>52</sup> Similar processes could possibly take place in the CB, which is enriched with PIWI proteins and piRNAs that are known to target other RNA species for degradation.<sup>14</sup> Indeed, our deep sequencing analysis revealed that the expression of a subset of mRNAs and CB-associated novel transcripts were misregulated in *Fyco1* cKO round spermatids. Interestingly, FYCO1 was also found to be localized in the late CB in elongating spermatids, where the abundance of vesicles associated with the late CB is even more prominent.<sup>53</sup> Therefore, the disruption of the CB-vesicle connection in *Fyco1* cKO testis may have even more apparent effects on transcriptomic balance later in development in elongating spermatids.

Interestingly, the integrity of the CB was compromised, and the CB was fragmented in several pieces in the absence of

FYCO1. It is currently unknown what causes the CB fragmentation, and one possibility is that detached fragments are normally degraded by FYCO1-mediated processes. However, FYCO1 may also augment the collection of smaller detached fragments back to the main CB structure. It is also possible that the FYCO1-mediated interplay between the CB and autophagosomes and lysosomes is involved in the maintenance of the CB integrity. The movements of the CB<sup>22</sup> and the vesicle transport are dependent on microtubule network. The fact that the disruption of the microtubule network causes similar fragmentation of the CB as *Fyco1* deletion (Fig. 5) suggests that microtubule-associated functions of FYCO1<sup>31,37</sup> are needed for the CB integrity. Identification of several kinesins as FYCO1-interacting proteins further highlights the importance of the microtubule network in FYCO1 function.

Because of the prominent molecular phenotype in *Fyco1* cKO round spermatids, it was somewhat unanticipated that the conditional inactivation of *Fyco1* gene in mice did not impair spermatogenesis and male fertility. In contrast, the deletion of any core components of the CB, such as PIWIL1, PIWIL2, DDX4, TDRD6 or TDRD7 (tudor domain containing 7), in mice results in spermatogenic failure and male infertility.<sup>7</sup> FYCO1 is consistently found in the mass spectrometry analysis of isolated CBs.<sup>12</sup> However, the current study showed that it appears not to be a core CB component, but localizes to the periphery of the CB and mediates the interaction of the CBs with vesicles and possibly with the microtubule network. Our results revealed that the presence of an intact single CB is not required for the progress of spermatogenesis but the RNA regulatory pathways remain functional when the CB is fragmented. This is in line with the studies on somatic RNP granules, the processing bodies (P-bodies), demonstrating that aggregation of P-body components into P-bodies is not required for their function but is instead a consequence of their activity.<sup>54</sup>

It is possible that in the absence of FYCO1, the disrupted interplay between the CB and vesicle trafficking is compensated by other, yet unidentified processes or homologous proteins. Interestingly, cellular defects in the *Fyco1* cKO germ cells were enhanced after challenging the cells in tubule culture conditions by autophagy inducers and inhibitors. Therefore, another option is that FYCO1-dependent processes are not required for the progress of spermatogenesis under physiological conditions, but become critical when the system is challenged by adverse conditions. Toxicological and aging-related mouse studies are in progress to clarify the potential role of FYCO1 in mediating stress-induced autophagy responses in spermatogenic cells.

Altogether, we revealed FYCO1 as a novel regulator of germ granules. Furthermore, our results provide the first molecular evidence on the factors that mediate the interplay between haploid male germ cell-specific RNP granules (CBs) and the autophagosome-lysosome system during spermatogenesis.

## Materials and methods

### Ethics statement

Mice were housed at the animal facility of the University of Turku, Finland, under controlled environmental conditions, following local laws and regulations (Finnish Act on the

Protection of Animals Used for Scientific or Educational Purposes [497/2013], Government Decree on the Protection of Animals Used for Scientific or Educational Purposes [564/2013]). Mice were sacrificed by CO<sub>2</sub> inhalation and cervical dislocation. The Laboratory Animal Care and Use Committee of the University of Turku approved all the animal experiments.

### Antibodies

Primary antibodies used in this study were: ACTA2/ $\alpha$  actin (sc-32251) and DDX25 (sc-51271) from Santa Cruz Biotechnology; TUBA/ $\alpha$  tubulin (MS-581-P1) from Thermo Fisher Scientific; DDX4 (ab13840), LAMP1 (ab25245), EIF4A3 (ab32485), RUVBL2 (ab36569) and DCP1A (ab47811) from Abcam; PIWIL1 (G82) and LC3B (2775) from Cell Signaling Technology; FYCO1 (H00079443-A01) from Abnova; FYCO1 (HPA035526 and SAB1400697) and RUVBL1 (HPA019948) from Sigma-Aldrich; GAPDH (5G4) from HyTest; PIWIL2 clone 13E-3 (MABE363) from Millipore. Rabbit polyclonal antibody against TSKS was a kind gift from Prof. J.A. Grootegoed, Department of Reproduction and Development, Erasmus MC - University Medical Center Rotterdam. Secondary antibodies conjugated with Alexa Fluor 488, 546, 594 and 647 made in donkey and streptavidin conjugated with Alexa Fluor 488 or 647 were purchased from Thermo Fisher Scientific (A-21202, A-21206, A-11055, A10036, A10040, A-11056, A-21203, A-21207, A-11058, A-31571, A-31573, A-21447, S32354, S32357). ECL anti-mouse IgG HRP-linked whole antibody made in sheep (NA931) and ECL anti-rabbit IgG HRP-linked made in donkey (NA934) were purchased from GE Healthcare Life Sciences.

### Electron microscopy and tomography

Samples were prepared as described previously.<sup>26</sup> Briefly, testis samples were fixed in 5% glutaraldehyde and treated with a potassium ferrocyanide-osmium fixative. The samples were embedded in epoxy resin (Glycidether 100, Merck), sectioned, post-stained with 5% uranyl acetate and 5% lead citrate, and visualized on a JEOL 1400 Plus transmission electron microscope (JEOL Ltd., Tokyo, Japan). Electron tomography samples were prepared following the same protocol except that uranyl acetate *en-bloc* staining was performed before plastic embedding. Serial semithick 220 nm sections were cut and placed on single slot grids. Colloidal gold particles of 10 nm in diameter were placed on top and below the grids to serve as markers for alignment of the tilt series. Dual axis tilt series were acquired using SerialEM software (<http://bio3b.colorado.edu/serialEM>) running on a Tecnai FEG 20 microscope (FEI, the Netherlands) operating at 200 kV. Images from 3 consecutive sections were recorded at 1-degree intervals over a tilt range of  $\pm 62$  degree. Tilt series were acquired using Ultrascan 4000 CCD camera (Gatan Corp., Pleasanton, CA, USA) at nominal magnification of 11.5 k providing a 2X binned pixel size of 1.94 nm. IMOD software (<http://bio3d.colorado.edu/imod>) was used to align the tilt series, and create 3D reconstructions. The images were segmented using Microscopy Image Browser, developed by the Electron Microscopy Unit, Institute of Biotechnology, University of Helsinki.<sup>55</sup> 3D rendering of selected cytoplasmic vesicles was performed with BioimageXD version 1.<sup>56</sup>

### Chromatoid body isolation

CB immunoprecipitation was performed as described previously.<sup>13</sup> Briefly, germ cells were released from 4 testes of adult C57BL/6 mice by digestion in 50 mg/mL Collagenase Type I (CLS-1, Worthington Biochemical Corporation) 0.1% w/v glucose in PBS and fixed in 0.1% paraformaldehyde (PFA) solution (Electron Microscopy Sciences, 15714). After fixation cells were lysed by sonication (UCD-200, Diagenode; medium settings, 30 sec with 30 sec pause) in 1.5 mL of RIPA buffer (50 mM Tris-HCl, pH 7.5, 1% Triton X-100 [Sigma, 93443], 0.5% w/v sodium deoxycholate [Sigma, D6750], 0.05% w/v sodium dodecyl sulfate [Sigma, 436143], 1 mM EDTA, 150 mM NaCl, 1X complete protease inhibition cocktail [Roche, 04693116001], 0.2 mM PMSF, 1 mM DTT) and the CB-enriched pellet fraction was obtained by centrifugation at  $300 \times g$  for 10 min. The CBs were immunoprecipitated using Dynabead Protein G (Thermo Fisher Scientific, 10003D) coupled to either anti-DDX4 antibody (Abcam, ab13840,) or rabbit IgG (Neo-markers, NC-100-P) at 4°C overnight with gentle mixing.

### Western blotting

Tissue samples were homogenized in RIPA lysis buffer containing 1 mM DTT, 0.2 mM PMSF and 1X protease inhibitor cocktail, and the lysates were cleared by centrifugation at  $14000 \times g$  for 5 min. For ontogenesis studies protein concentration was measured using Pierce BCA protein assay kit (Life Technologies, 23227); absorbance was measured with a Victor2 plate reader (Wallac, Turku, Finland). Samples diluted in Laemmli buffer were incubated 5 min at 95°C before loading them on the gel. Samples were run at 100 V and then transferred to a PVDF membrane (Amersham, RPN303F) with wet-blotting system (Bio-Rad) at 90 V for 1 h at 4°C. After blotting the PVDF membrane was incubated in 100% methanol for 15 seconds and air-dried for 30 min at 37°C or at room temperature overnight. The membrane was then incubated with primary antibody diluted in 5% skimmed-milk, 0.1% Triton X-100 (Sigma, 93443) in phosphate-buffered saline (PBS; 137 mM NaCl, 2.7 mM KCl, 10 mM Na<sub>2</sub>HPO<sub>4</sub>, 1.8 mM KH<sub>2</sub>PO<sub>4</sub>, pH 7.4) (blocking solution) for 1 h at room temperature, washed  $3 \times 5$  min with 0.1% Triton X-100 in PBS (PBST), incubated with secondary antibody diluted 1:1000 in blocking solution, washed  $5 \times 5$  min in PBST, and incubated 1 min with Western Lightning ECL Pro (Perkin Elmer, NEL121001EA). The chemiluminescence signal was recorded using LAS4000 (Fujifilm) as 16 bit .TIFF files. Band intensity was measured using ImageJ software. The band intensities from actin and tubulin were used for normalization. The results represent the mean of biological duplicates.

### RT-qPCR

RNA was isolated from FVB mouse testis at different time points postpartum or enriched populations of round spermatids with TRIsure (BIO-38033, Biotline) following the manufacturer's instructions. RNA was resuspended in MilliQ water to a final concentration of 1  $\mu\text{g}/\mu\text{L}$ . Before cDNA synthesis, 1  $\mu\text{g}$  of RNA per sample was treated with DNase I (Sigma-Aldrich, AMPD1). cDNA was synthesized with DyNAmo cDNA Synthesis Kit (Thermo Scientific, F-470) following the manufacturer's instructions using 1  $\mu\text{g}$  of RNA as a template. The reverse transcription

reaction was then resuspended 1:20 in MilliQ water for qPCR. qPCR was performed with the DyNAmo HS SYBR Green qPCR kit (Thermo Scientific, F-410) following the manufacturer's instructions. *Ppia*, *Actb* and *Rplp0* (for *Fyco1* ontogenesis) or *Ppia* and *Rpl19* (for sequencing validation) were used as reference genes. All reactions were performed on either a CFX96 or CFX384 Real Time qPCR detection system (Bio-Rad, Hercules, CA, USA). The geometric mean of the Ct values from the reference genes was used as a normalization factor for the calculation of the delta-Ct for each gene of interest at each sample. The delta-delta-Ct value was calculated using the 1-w time point (*Fyco1* ontogenesis) or control round spermatids (sequencing validation) as reference. Either 2 (sequencing validation) or 3 (*Fyco1* ontogenesis) biological replicates were analyzed. All RT-qPCR reactions and analysis were performed following MIQE guidelines. Further information (quality control of RNA template, validation of primers and reference genes, primer sequences) is available upon request.

### Preparation of germ cells and tissues for immunostaining

Squash slides of stage specific sections of mouse seminiferous tubules were prepared as described earlier.<sup>57</sup> Briefly, testes from FVB or C57BL/6 adult mice were decapsulated and sections representing specific stages of the seminiferous epithelium were isolated based on the light absorption pattern with the help of a stereomicroscope. The sections of the seminiferous tubules were then transferred to a glass slide with the use of a pipette and a glass coverslip deposited on top of the tubule section to allow the germ cells to spread out from the tubule. Once the germ cells formed a monolayer, the glass slide was snap-frozen in liquid nitrogen and, after quickly removing the coverslip, fixed in 100% ice-cold acetone for 10 min and air-dried overnight at room temperature. Slides were postfixed in 4% paraformaldehyde in PBS for 10 min, washed 5 min in PBS, incubated 5 min in 0.2% Triton X-100 in PBS and washed 3 × 5 min in PBS before starting with IF staining.

For paraffin embedding, testes collected from FVB or C57BL/6 adult mice were fixed in 4% PFA in PBS overnight at room temperature. Testes were washed in milliQ water for 2 h with repeated changes of fresh milliQ water, incubated 2 × 30 min in 50% ethanol and 2 × 30 min in 70% ethanol before embedding in paraffin. Paraffin-embedded testis sections were deparaffinized by incubation 3 × 5 min in xylene, 2 × 10 min in 100% ethanol, 2 × 10 min in 96% ethanol, 2 × 10 min in 70% ethanol and then washed in milliQ water 2 × 2 min. Antigen retrieval was performed by incubation in sodium citrate solution (10 mM sodium citrate, 0.05% Tween 20 [Sigma, P2287], pH 6.0) or in Tris-EDTA solution (10 mM Tris Base, 1 mM EDTA Solution, 0.05% Tween 20, pH 9.0) for 20 min, at 1 atmosphere at 120°C. After cooling down to room temperature for at least 2 h slides were washed 4 × 3 min in milliQ water and 5 min in PBS before starting with IF staining.

### Immunofluorescence

Slides were incubated with 10% normal donkey serum (Jackson ImmunoResearch, 017-000-121) and 3% bovine serum albumin (Sigma, A2153) in PBST (blocking solution) for 1 h. Primary antibody was diluted in blocking solution and incubation was performed for 1 h at room temperature or overnight at 4°C. Slides

were washed 3 × 5 min with PBST. Secondary antibody was diluted 1:1000 in blocking solution and incubation performed for 1 h at room temperature. Blocking and incubation with antibody solutions were performed in a humidified environment protected from light. Slides were washed 3 × 5 min in PBST, incubated 5 min in DAPI (Sigma-Aldrich, D9542; 5 mg/mL stock) diluted 1:20,000 in PBS, washed 5 min in PBS followed by 5 min with milliQ water and finally mounted with Vectashield HardSet Mounting Medium (Vector Laboratories, H-1400) or ProLong Diamond Antifade Mountant (Life Technologies, P36970). Slides were left for 24 h at room temperature for the mounting medium to solidify.

### Imaging

Widefield fluorescence images were acquired with Zeiss Axio Imager M1 microscope (Oberkochen, Germany) equipped with an AxioCam MRc camera using a 40X/0.75 DIC Plan-NeoFluar objective. Widefield images were acquired and processed for publication with Zeiss Zen 2011 software. Confocal images were acquired using either a Zeiss 510 META or Zeiss 780 laser scanning confocal microscope (Oberkochen, Germany) with 40X/1.2 Water or 100X/1.4 Oil DIC objective. Resolution in the 3 dimensions was set at optimal with Zeiss Zen 2011 software. Confocal images were analyzed and modified for publication (background subtraction, contrast and brightness adjustment) with BioimageXD version 1.0<sup>56</sup> or with ImageJ software. 3D model reconstruction was performed using Slidebook 6 reader, version 6.0.4 (24366) (3i). All IF figures represent confocal images unless otherwise stated in the figure legends.

### Seminiferous tubule cultures

For immunofluorescence analysis rapamycin (Santa Cruz Biotechnology, sc-3504) and nocodazole (Sigma, M1404) were diluted 10 mg/mL in DMSO. Baf (Santa Cruz Biotechnology, sc-201550) was diluted 0.1 mg/mL in DMSO. Wortmannin (Sigma, W1628) was diluted to 0.12 mM in DMSO. Sections of the seminiferous tubules representing stage II-V of the seminiferous epithelial cycle were dissected as described above and cultured in 50 μL final volume of DMEM with drug or vehicle alone diluted 1:100 for 6 h in a humidified incubator at 34°C, 5% CO<sub>2</sub>. After incubation, squash slides were prepared, and samples were labeled for IF as described above. For protein expression quantification, sections of seminiferous tubules were cultured in 500 μM rapamycin, 5 μM Baf or vehicle alone for 6 h in a humidified incubator at 34°C, 5% CO<sub>2</sub>. Tubules were collected by centrifugation 500 × g, 5 min in 4°C, homogenized with a TissueLyser LT (Qiagen, Hilden, Germany) 50 Hz for 30 seconds in RIPA buffer. Cells were left to lyse 30 min on ice, centrifuged as before and supernatant analyzed by western blot analysis as described. Band intensity was measured using ImageJ software. GAPDH was used for normalization. The results represent the mean of biological triplicates with s.e.m and 2-tailed *t* test performed by GraphPad Prism 7.00 software.

### Isolation of germ cells

Testes from 2 C57Bl/6J adult mice were collected in PBS, transferred in 8 mL 1X KREBS buffer (25 mM NaHCO<sub>3</sub>, 1.2 mM

$\text{KH}_2\text{PO}_4$ , 120 mM NaCl, 1.2 mM  $\text{MgSO}_4 \cdot 7\text{H}_2\text{O}$ , 11.10 mM dextrose, 1.3 mM  $\text{CaCl}_2 \cdot 2\text{H}_2\text{O}$ , 4.8 mM KCl, pH 7.4),<sup>58</sup> tunica albuginea was removed and seminiferous tubules were minced with scissors. The solution containing the seminiferous tubule fragments was divided into 2 tubes containing 25 mL collagenase solution (1X KREBS buffer with 22.5 mg collagenase type I [Worthington Biochemical Corporation, LS004194]) each prewarmed at 34°C. Cells in collagenase solution were incubated at 34°C for 10 min in rotation. Cell suspensions were centrifuged 2 min, 500 × *g* at room temperature, supernatant was discarded and each pellet (composed of germ cells and seminiferous tubule fragments) was resuspended in 25 mL trypsin solution (1X KREBS buffer with 15 mg trypsin [Worthington Biochemical Corporation, LS003708] and 5 μg DNase I [Sigma-Aldrich, DN25]) prewarmed at 34°C. Cell suspensions in trypsin solution were incubated at 34°C for 10 min in rotation. Cell suspensions were mixed 10 times with a wide bore pipette. 5 μg DNase I were added to each cell suspension and again incubated at 34°C for 10 min in rotation. After 2 min, 500 × *g* centrifugation at RT, the cell pellets were resuspended in 25 mL 1X KREBS buffer and filtered through 100 μm filter. Cell suspensions were pooled together and centrifuged 2 min, 500 × *g* at RT. Cell pellet was resuspended in 5 mL ice-cold 1X KREBS buffer. Cell suspension was loaded on the top of an ice-cold discontinuous BSA density gradient (1–2–3–4–5–6% BSA in 1X KREBS, 5 mL each) in a 50 mL tube. Cells were allowed to sediment for 1.5 h at 4°C. 1 mL fractions were collected starting from the top of the gradient, centrifuged 5 min at 500 × *g*, washed twice with ice-cold 1X KREBS buffer and stored on ice. 5 μL of each fraction were diluted in 10 μL fixing solution (4% PFA, 0.05% Triton X-100) with DAPI (Sigma-Aldrich, D9542; diluted 1:20,000 from 5 mg/mL stock solution). Each fraction was analyzed by DAPI staining and fluorescence microscopy for the enrichment in round spermatids.

### RNA sequencing and data analysis

Total RNA was isolated from round spermatids using TRIpure (Bioline, BIO-38033) following the manufacturer's instructions. RNA samples were further processed at the Finnish Microarray and Sequencing Center at the Turku Center for Biotechnology. Poly-A RNA was enriched using standard procedures and sequencing was performed using a HiSeq 3000 sequencing system (Illumina, San Diego, CA, USA). Two control and 2 cKO samples were submitted for sequencing. Transcript analysis was performed using the *Mus musculus* genome as a reference (Ensembl built 82). Mapping of the transcripts was performed using STAR (Version 2.4.2a). Fragments per kilobase of transcript per million mapped reads quantification was performed with RSEM (Version 1.2.22) and count data was obtained with HTSeq (Version 0.6.1p1). Differential expression (DE) analysis was performed using the edgeR package.<sup>59</sup> We used piRNA precursor coordinates from Li et al.<sup>60</sup> and the coordinates for CB-associated novel transcripts were from Meikar et al.<sup>12</sup> Nonexpressed genes were filtered from the data. Only genes with at least 2 counts per million mapped reads were considered for quantification analysis. TMM normalization was applied to account for the compositional bias. Transposons were quantified using the piPipes pipeline that uses the RepBase database for the transposon sequence information.<sup>61</sup> Cufflinks and Cuffmerge (Version 2.1.1)<sup>62</sup> were used to predict novel intergenic transcripts. Individual counts for the consensus loci were again

obtained using HTSeq and the DE analysis was then performed with the edgeR package.

### Preparation of testicular vesicle fraction

Testes from 3 C57Bl/6J adult mice were collected, tunica albuginea was removed and seminiferous tubules were minced with scissors. The solution containing the seminiferous tubule fragments was divided into 2 tubes containing 25 mL collagenase solution (0.1% glucose in PBS with 22.5 mg collagenase type I and 5 μg DNase I). Cells in collagenase solution were incubated at 34°C for 30 min with gentle shaking. Cells were centrifuged 5 min 500 × *g* at 4°C and the cell pellets washed twice with ice cold 0.1% glucose PBS. Cells were combined to one tube and after a final 500 × *g* at 4°C centrifugation, supernatant was discarded and 1,500 μl of HEPES buffer (0.25 M sucrose, 10 mM HEPES, pH 7.2, 1X complete protease inhibitor cocktail) was added. Cells were disrupted by nitrogen cavitation (Parr Instruments, 500 p.s.i, 5 min at room temperature). Cell lysate was centrifuged 5 min, 17,000 × *g* at 4°C. FYCO1 complexes were immunoprecipitated using Dynabead Protein G coupled to either rabbit anti-FYCO1 antibody (Sigma) or rabbit IgG at 4°C overnight.

### Cell culture

HeLa cells (American Type Culture Collection, CCL-2) were cultured in Dulbecco's Modified Eagle's Medium (DMEM)/F12 media (Gibco) supplemented with 10% fetal calf serum (FCS; PromoCell), 50 IU/ml penicillin and 50 μg/ml streptomycin supplemented at 37°C in humidified atmosphere with 5% CO<sub>2</sub>. To induce autophagy, cells were amino acid- and serum-starved for 1 h. Cells were collected, lysed with RIPA buffer and cell debris pelleted by centrifugation (17,000 × *g*, 5 min, 4°C). Supernatant diluted with Laemmli buffer was used in western blot analysis as described before.

### Immunoprecipitation

Four testes from adult mice were collected in PBS. Seminiferous tubules were released from the tunica albuginea, quickly minced with scissors and incubated 60–90 min at RT in 50 mL of collagenase solution (0.5 mg/mL collagenase type I, 0.1% glucose in PBS) in rotation to release the germ cells from the seminiferous tubules. The cell suspension was centrifuged 5 min, 500 × *g* at 4°C. The pellet was resuspended in ice-cold 50 mL 0.1% glucose in PBS, filtered through a 100-μm filter to eliminate pieces of seminiferous tubules and centrifuged again. Cells were lysed on ice for 30 min in 1 mL isotonic nondenaturing lysis buffer (150 mM NaCl, 5 mM EDTA, 50 mM Tris-HCl, pH 8.0, 1% Triton X-100, 1X complete mini mix [Roche, 4693124001], 0.2 mM PMSF and 1 mM DTT). Samples were centrifuged 10 min, 500 × *g* at 4°C to eliminate cellular debris and intact chromatoid bodies. FYCO1 complexes were immunoprecipitated using Dynabead Protein G coupled to either rabbit anti-FYCO1 antibody (Sigma) or rabbit IgG at 4°C overnight.

### Mass spectrometry

To remove Triton X-100, beads were washed 2 × 1 mL of 25 mM NH<sub>4</sub>HCO<sub>3</sub> buffer and 2 × 200 μL of 6 M urea in

25 mM  $\text{NH}_4\text{HCO}_3$  buffer. Samples were loaded on a Criterion XT Bis-Tris precast 12% SDS-PAGE gel (Bio-Rad) and run with constant 200 V for 9 min. MOPS buffer was used as a running buffer. Three pieces from the upper part of the SDS-PAGE gel were cut and samples were in-gel digested at the Turku Proteomics Facility according to the standard protocol. Digested peptides were dissolved in 1% formic acid (ctrl 11  $\mu\text{L}$  and all the rest 15  $\mu\text{L}$ ). Samples (5  $\mu\text{L}$ ) were submitted to LC-ESI-MS/MS analysis. The LC-ESI-MS/MS analyses were performed on a nanoflow HPLC system (Easy-nLCII, Thermo Fisher Scientific, Waltham, MA, USA) coupled to the LTQ Orbitrap Velos Pro mass spectrometer (Thermo Fisher Scientific, Bremen, Germany) equipped with a nano-electrospray ionization source. Peptides were first loaded on a trapping column and subsequently separated inline on a 15-cm C18 column (75  $\mu\text{m} \times 15 \text{ cm}$ , Magic 5  $\mu\text{m}$  200 Å C18, Michrom BioResources Inc., Sacramento, CA, USA). The mobile phase consisted of water/acetonitrile (98:2 [v/v]) with 0.2% formic acid (solvent A) and acetonitrile/water (95:5 [v/v]) with 0.2% formic acid (solvent B). A linear 30 min gradient from 5% to 35% B was used to elute peptides. MS data was acquired automatically by using Thermo Xcalibur 3.0 software (Thermo Fisher Scientific). An information dependent acquisition method consisted of an Orbitrap MS survey scan of mass range 300 to 2000  $m/z$ . The data files were searched for protein identification using Proteome Discoverer 1.4 software (Thermo Fisher Scientific) connected to an in-house Mascot server running the Mascot 2.4.1 software (Matrix Science). Data were searched against the SwissProt database (release 2014\_08). The following search parameters were used. Type of search: MS/MS Ion Search, Taxonomy: *Mus musculus*, Enzyme: Trypsin, Fixed modifications: Carbamidomethyl (C), Variable modifications: Oxidation (M), Mass values: Monoisotopic, Peptide Mass Tolerance:  $\pm 5$  ppm, Fragment, Mass Tolerance:  $\pm 0.5$  Da, Max Missed Cleavages: 1, Instrument type: ESI-TRAP. Results from ProteomeDiscoverer were exported and saved as Excel files. Only proteins assigned at least with 2 peptides were accepted.

### Generation of *Fyco1* conditional knockout mice

The genetic background of all the mice used in this study was mixed background with C57Bl/6J and SV129. The construct for the generation of the *Fyco1* conditional knockout (MGI:107277) was purchased from the International Mouse Phenotyping Consortium, and validity of construct was confirmed by restriction enzyme digestion and by sequencing. G4 embryonic stem cells (ES, derived from 129S6/C57BL/6Ncr mice) were cultured on neomycin-resistant primary embryonic fibroblast feeder layers, and  $10^6$  cells were electroporated with 30  $\mu\text{g}$  of linearized targeting construct. After electroporation, the cells were plated on 100 mm culture dishes and exposed to G418 (300  $\mu\text{g}/\text{ml}$ ; Sigma). Colonies were picked up after 7 to 9 d of selection, and grown on 96-well plates. In order to delete *Neo* cassette in the targeted ES cells, they were re-electroporated with plasmid pCAGGS-*Cre* and plated on 100 mm culture dishes. Colonies were picked up after 3 to 5 d growth and grown on 96-well plates. Targeted ES clones and ES clones with *Neo* deletion were detected by LR-PCR and PCR, and right PCR products were further confirmed by sequencing. The right

targeted ES clones with *Neo* deletion were used for blastocyst injection and for creation of chimera. Male chimeras were bred with wild-type females to determine the germline transmission. To achieve selective inactivation of *Fyco1* in germ cells, transgenic *Neurog3 Cre* mice<sup>63</sup> were mated with homozygous *Fyco1* floxed alleles, *Fyco1*<sup>(*fx/fx*)</sup> in order to generate *Fyco1*<sup>(*fx/wt*)</sup>; *Neurog3 Cre*<sup>+</sup> and *Fyco1*<sup>(*fx/wt*)</sup>; *Neurog3 Cre*<sup>-</sup> mice. These animals were then intercrossed to produce *Fyco1*<sup>(*fx/fx*)</sup>; *Neurog3 Cre*<sup>+</sup>, and *Fyco1*<sup>(*fx/fx*)</sup>; *Neurog3 Cre*<sup>-</sup>, and *Fyco1*<sup>(*fx/wt*)</sup>; *Neurog3 Cre*<sup>-</sup> littermates. *Cre*-mediated recombination was detected and confirmed by PCR with different primer pairs. Further information (validation of primers, primer sequences) is available upon request.

### Histology and morphological analysis of spermatozoa

For histological analyses, tissues were collected and directly fixed in 4% PFA or in Bouin fixative (4 to 20 h at room temperature). Tissues were then dehydrated in a series of ethanol washes as described above and embedded in paraffin. Paraffin embedded tissues were cut and stained with hematoxylin and eosin (HE) or periodic acid-Schiff (PAS) according to standard protocols. Epididymal sperm was released in PBS from cauda epididymis and spread on glass slides, air-dried and stained with hematoxylin for morphological analysis.

### Statistical analyses

For colocalization studies, Manders coefficients were calculated using BioimageXD and data analysis was done using MS Excel 2016. For other data analyses, the Graphpad Prism 7 (GraphPad Software Inc., LaJolla, CA, USA) was used. *P* values  $\leq 0.05$  were considered significant.

### Abbreviations

Baf	bafilomycin A <sub>1</sub>
CB	chromatoid body
cKO	conditional knockout
DDX25	DEAD (Asp-Glu-Ala-Asp) box polypeptide 25
DDX4	DEAD (Asp-Glu-Ala-Asp) box polypeptide 4
DE	differentially expressed
EM	electron microscopy
FYCO1	FYVE and coiled-coil domain containing 1
GO	gene ontology
LAMP1	lysosomal-associated membrane protein 1
LC3	microtubule-associated protein 1 light chain 3
piRNA	PIWI-interacting RNA
PIWI	P-element-induced <i>wimpy</i> testis
PIWIL1	piwi-like RNA-mediated gene silencing 1
PIWIL2	piwi-like RNA-mediated gene silencing 2
RNP	ribonucleoprotein
TDRD6	tudor domain containing 6
TSKS	testis specific serine kinase substrate

### Disclosure of potential conflicts of interest

No potential conflicts of interest were disclosed.

## Acknowledgements

We are grateful to Dr. Shinichiro Chuma (Kyoto University, Japan) for *tdrd6* knockout testis cryoblocks, Dr. Gregory Hannon (CSHL, USA) for *piwil1* knockout testis samples and Prof. J.A. Grootegoed (University Medical Center Rotterdam) for the anti-TSKS antibody. We would like to thank the Turku Center for Biotechnology Cell Imaging Core, Proteomics Facility and Finnish Microarray and Sequencing Center, as well as the EM unit of the University of Turku for their services. The Turku Center for Disease Modeling (TCDM) is acknowledged for the generation of the *Fycy1* cKO mouse line and the Turku Central Animal Facility for housing the animals.

## Funding

This study was supported by the Academy of Finland, the Sigrid Jusélius Foundation, the Novo Nordisk Foundation, the Turku Doctoral Program of Biomedical Sciences, the Turku Doctoral Program of Molecular Medicine, the Finnish Cultural Foundation, the Turku University Hospital, and the Turku University Foundation.

## References

- Soumillon M, Necsulea A, Weier M, Brawand D, Zhang X, Gu H, Barthès P, Kokkinaki M, Nef S, Gnirke A, et al. Cellular source and mechanisms of high transcriptome complexity in the mammalian testis. *Cell Rep* 2013; 3:2179-90; PMID:23791531; <http://dx.doi.org/10.1016/j.celrep.2013.05.031>
- Chalmel F, Lardenois A, Evrard B, Rolland AD, Sallou O, Dumargne MC, Coiffec I, Collin O, Primig M, Jégou B. High-resolution profiling of novel transcribed regions during rat spermatogenesis. *Biol Reprod* [Internet] 2014 [cited 2015 Feb 25]; 91:5. Available from: <http://www.ncbi.nlm.nih.gov/pubmed/24740603>
- Laiho A, Kotaja N, Gyenesei A, Sironen A. Transcriptome profiling of the murine testis during the first wave of spermatogenesis. *PLoS One* [Internet] 2013; 8:e61558. Available from: <http://www.pubmedcentral.nih.gov/articlerender.fcgi?artid=3629203&tool=pmcentrez&rendertype=abstract>; <http://dx.doi.org/10.1371/journal.pone.0061558>
- Idler RK, Yan W. Control of messenger RNA fate by RNA-binding proteins: an emphasis on mammalian spermatogenesis. *J Androl* 2012; 33:309-37; PMID:21757510; <http://dx.doi.org/10.2164/jandrol.111.014167>
- Paronetto MP, Sette C. Role of RNA-binding proteins in mammalian spermatogenesis. *Int J Androl* 2010; 33:2-12; PMID:19281489; <http://dx.doi.org/10.1111/j.1365-2605.2009.00959.x>
- Gao M, Arkov AL. Next generation organelles: structure and role of germ granules in the germline. *Mol Reprod Dev* [Internet] 2013 [cited 2015 Jun 25]; 80:610-23. Available from: <http://www.pubmedcentral.nih.gov/articlerender.fcgi?artid=3584238&tool=pmcentrez&rendertype=abstract>
- Meikar O, Da Ros M, Korhonen H, Kotaja N. Chromatoid body and small RNAs in male germ cells. *Reproduction* 2011; 142:195-209; PMID:21652638; <http://dx.doi.org/10.1530/REP-11-0057>
- Kotaja N, Sassone-Corsi P. The chromatoid body: a germ-cell-specific RNA-processing centre. *Nat Rev Mol Cell Biol* 2007; 8:85-90; PMID:17183363; <http://dx.doi.org/10.1038/nrm2081>
- Fawcett DW, Eddy EM, Phillips DM. Observations on the fine structure and relationships of the chromatoid body in mammalian spermatogenesis. *Biol Reprod* 1970; 2:129-53; PMID:4106274; <http://dx.doi.org/10.1095/biolreprod.2.1.129>
- Shang P, Baarends WM, Hoogerbrugge J, Ooms MP, van Cappellen WA, de Jong AAW, Dohle GR, van Eenennaam H, Gossen JA, Grootegoed JA. Functional transformation of the chromatoid body in mouse spermatids requires testis-specific serine/threonine kinases. *J Cell Sci* 2010; 123:331-9; PMID:20053632; <http://dx.doi.org/10.1242/jcs.059949>
- Meikar O, Da Ros M, Liljenbäck H, Toppari J, Kotaja N. Accumulation of piRNAs in the chromatoid bodies purified by a novel isolation protocol. *Exp Cell Res* 2010; 316:1567-75; PMID:20219458; <http://dx.doi.org/10.1016/j.yexcr.2010.02.023>
- Meikar O, Vagin V V, Chalmel F, Söstar K, Lardenois A, Hammell M, Jin Y, Da Ros M, Wasik KA, Toppari J, et al. An atlas of chromatoid body components. *RNA* [Internet] 2014 [cited 2014 Apr 28]; 20:483-95. Available from: <http://www.ncbi.nlm.nih.gov/pubmed/24554440>; <http://dx.doi.org/10.1261/rna.043729.113>
- Meikar O, Kotaja N. Isolation of chromatoid bodies from mouse testis as a rich source of short RNAs. *Methods Mol Biol* [Internet] 2014 [cited 2015 May 25]; 1173:11-25. Available from: <http://www.ncbi.nlm.nih.gov/pubmed/24920356>; [http://dx.doi.org/10.1007/978-1-4939-0931-5\\_2](http://dx.doi.org/10.1007/978-1-4939-0931-5_2)
- Siomi MCMC, Sato K, Pezic D, Aravin AAA. PIWI-interacting small RNAs: the vanguard of genome defence. *Nat Rev Mol Cell Biol* 2011; 12:246-58; PMID:21427766; <http://dx.doi.org/10.1038/nrm3089>
- Pezic D, Manakov SA, Sachidanandam R, Aravin AA. piRNA pathway targets active LINE1 elements to establish the repressive H3K9me3 mark in germ cells. *Genes Dev* [Internet] 2014 [cited 2015 Jun 25]; 28:1410-28. Available from: <http://www.pubmedcentral.nih.gov/articlerender.fcgi?artid=4083086&tool=pmcentrez&rendertype=abstract>; <http://dx.doi.org/10.1101/gad.240895.114>
- Aravin AAA, Sachidanandam R, Bourc'his D, Schaefer C, Pezic D, Toth KFKF, Bestor T, Hannon GJGJ. A piRNA pathway primed by individual transposons is linked to de novo DNA methylation in mice. *Mol Cell* 2008; 31:785-99; PMID:18922463; <http://dx.doi.org/10.1016/j.molcel.2008.09.003>
- Kuramochi-Miyagawa S, Watanabe T, Gotoh K, Totoki Y, Toyoda A, Ikawa M, Asada N, Kojima K, Yamaguchi Y, Ijiri TW, et al. DNA methylation of retrotransposon genes is regulated by Piwi family members MIL1 and MIWI2 in murine fetal testes. *Genes Dev* 2008; 22:908-17; PMID:18381894; <http://dx.doi.org/10.1101/gad.1640708>
- Goh WSS, Falcatori I, Tam OH, Burgess R, Meikar O, Kotaja N, Hammell M, Hannon GJ. piRNA-directed cleavage of meiotic transcripts regulates spermatogenesis. *Genes Dev* [Internet] 2015 [cited 2015 May 20]; 29:1032-44. Available from: <http://www.ncbi.nlm.nih.gov/pubmed/25995188>; <http://dx.doi.org/10.1101/gad.260455.115>
- Gou LT, Dai P, Yang JH, Xue Y, Hu YP, Zhou Y, Kang JY, Wang X, Li H, Hua MM, et al. Pachytene piRNAs instruct massive mRNA elimination during late spermiogenesis. *Cell Res* 2014; 24:680-700; PMID:24787618; <http://dx.doi.org/10.1038/cr.2014.41>
- Zhang P, Kang JY, Gou LT, Wang J, Xue Y, Skogerboe G, Dai P, Huang DW, Chen R, Fu XD, et al. MIWI and piRNA-mediated cleavage of messenger RNAs in mouse testes. *Cell Res* [Internet] 2015 [cited 2015 Jun 25]; 25:193-207. Available from: <http://www.ncbi.nlm.nih.gov/pubmed/25582079>; <http://dx.doi.org/10.1038/cr.2015.4>
- Watanabe T, Cheng E, Zhong M, Lin H. Retrotransposons and pseudogenes regulate mRNAs and lncRNAs via the piRNA pathway in the germline. *Genome Res* [Internet] 2015 [cited 2015 Jun 25]; 25:368-80. Available from: <http://www.ncbi.nlm.nih.gov/pubmed/25480952>; <http://dx.doi.org/10.1101/gr.180802.114>
- Ventela S, Toppari J, Parvinen M, Ventelä S, Toppari J, Parvinen M. Intercellular organelle traffic through cytoplasmic bridges in early spermatids of the rat: mechanisms of haploid gene product sharing. *Mol Biol Cell* 2003; 14:2768-80; PMID:12857863; <http://dx.doi.org/10.1091/mbc.E02-10-0647>
- Parvinen M, Jokelainen PT. Rapid movements of the chromatoid body in living early spermatids of the rat. *Biol Reprod* 1974; 11:85-92; PMID:4616728; <http://dx.doi.org/10.1095/biolreprod11.1.85>
- Parvinen M, Salo J, Toivonen M, Nevalainen O, Soini E, Pelliniemi LJ. Computer analysis of living cells: movements of the chromatoid body in early spermatids compared with its ultrastructure in snap-frozen preparations. *Histochem Cell Biol* 1997; 108:77-81; PMID:9377227; <http://dx.doi.org/10.1007/s004180050148>
- Soderstrom KO, Parvinen M. Transport of material between the nucleus, the chromatoid body and the Golgi complex in the early spermatids of the rat. *Cell Tissue Res* 1976; 168:335-42; PMID:1277272; <http://dx.doi.org/10.1007/BF00215311>
- Da Ros M, Hirvonen N, Olotu O, Toppari J, Kotaja N. Retromer vesicles interact with RNA granules in haploid male germ cells. *Mol Cell Endocrinol* [Internet] 2015 [cited 2015 May 25]; 401:73-83. Available from: <http://www.ncbi.nlm.nih.gov/pubmed/25486514>; <http://dx.doi.org/10.1016/j.mce.2014.11.026>

- [27] Buchan JR, Kolaitis RM, Taylor JP, Parker R. Eukaryotic stress granules are cleared by autophagy and Cdc48/VCP function. *Cell* [Internet] 2013 [cited 2014 Jul 25]; 153:1461-74. Available from: <http://www.pubmedcentral.nih.gov/articlerender.fcgi?artid=3760148&tool=pmcentrez&rendertype=abstract>; <http://dx.doi.org/10.1016/j.cell.2013.05.037>
- [28] Ryu HH, Jun MH, Min KJ, Jang DJ, Lee YS, Kim HK, Lee JA. Autophagy regulates amyotrophic lateral sclerosis-linked fused in sarcoma-positive stress granules in neurons. *Neurobiol Aging* [Internet] 2014 [cited 2015 Jun 9]; 35:2822-31. Available from: <http://www.ncbi.nlm.nih.gov/pubmed/25216585>; <http://dx.doi.org/10.1016/j.neurobiolaging.2014.07.026>
- [29] Seguin SJ, Morelli FF, Vinet J, Amore D, De Biasi S, Poletti A, Rubinsztein DC, Carra S. Inhibition of autophagy, lysosome and VCP function impairs stress granule assembly. *Cell Death Differ* [Internet] 2014 [cited 2015 Apr 28]; 21:1838-51. Available from: <http://www.pubmedcentral.nih.gov/articlerender.fcgi?artid=4227144&tool=pmcentrez&rendertype=abstract>; <http://dx.doi.org/10.1038/cdd.2014.103>
- [30] Mizushima N, Komatsu M. Autophagy: renovation of cells and tissues. *Cell* [Internet] 2011 [cited 2016 May 27]; 147:728-41. Available from: <http://www.ncbi.nlm.nih.gov/pubmed/22078875>; <http://dx.doi.org/10.1016/j.cell.2011.10.026>
- [31] Pankiv S, Alemu EA, Brech A, Bruun JA, Lamark T, Overvatn A, Bjorkoy G, Johansen T. FYCO1 is a Rab7 effector that binds to LC3 and PI3P to mediate microtubule plus end-directed vesicle transport. *J Cell Biol* 2010; 188:253-69; PMID:20100911; <http://dx.doi.org/10.1083/jcb.200907015>
- [32] Olsvik HL, Lamark T, Takagi K, Larsen KB, Evjen G, Overvatn A, Mizushima T, Johansen T. FYCO1 Contains a C-terminally Extended, LC3A/B-preferring LC3-interacting Region (LIR) Motif Required for Efficient Maturation of Autophagosomes during Basal Autophagy. *J Biol Chem* [Internet] 2015 [cited 2016 Jun 5]; 290:29361-74. Available from: <http://www.ncbi.nlm.nih.gov/pubmed/26468287>; <http://dx.doi.org/10.1074/jbc.M115.686915>
- [33] Cheng X, Wang Y, Gong Y, Li F, Guo Y, Hu S, Liu J, Pan L. Structural basis of FYCO1 and MAP1LC3A interaction reveals a novel binding mode for Atg8-family proteins. *Autophagy* [Internet] 2016 [cited 2016 Jun 5]; 12(8):1330-9. Available from: <http://www.ncbi.nlm.nih.gov/pubmed/27246247>
- [34] Shpilka T, Weidberg H, Pietrokovski S, Elazar Z. Atg8: an autophagy-related ubiquitin-like protein family. *Genome Biol* [Internet] 2011 [cited 2016 May 14]; 12:226. Available from: <http://www.pubmedcentral.nih.gov/articlerender.fcgi?artid=3218822&tool=pmcentrez&rendertype=abstract>; <http://dx.doi.org/10.1186/gb-2011-12-7-226>
- [35] Ma J, Becker C, Reyes C, Underhill DM. Cutting edge: FYCO1 recruitment to dectin-1 phagosomes is accelerated by light chain 3 protein and regulates phagosome maturation and reactive oxygen production. *J Immunol* [Internet] 2014 [cited 2016 Jun 5]; 192:1356-60. Available from: <http://www.pubmedcentral.nih.gov/articlerender.fcgi?artid=3966112&tool=pmcentrez&rendertype=abstract>; <http://dx.doi.org/10.4049/jimmunol.1302835>
- [36] Mrakovic A, Kay JG, Furuya W, Brumell JH, Botelho RJ. Rab7 and Arl8 GTPases are necessary for lysosome tubulation in macrophages. *Traffic* [Internet] 2012 [cited 2016 Jun 5]; 13:1667-79. Available from: <http://www.ncbi.nlm.nih.gov/pubmed/22909026>; <http://dx.doi.org/10.1111/tra.12003>
- [37] Raiborg C, Wenzel EM, Pedersen NM, Olsvik H, Schink KO, Schultz SW, Vietri M, Nisi V, Bucci C, Brech A, et al. Repeated ER-endosome contacts promote endosome translocation and neurite outgrowth. *Nature* 2015; 520:234-8; PMID:25855459; <http://dx.doi.org/10.1038/nature14359>
- [38] Wymann MP, Bulgarelli-Leva G, Zvebil MJ, Pirola L, Vanhaesebroeck B, Waterfield MD, Panayotou G. Wortmannin inactivates phosphoinositide 3-kinase by covalent modification of Lys-802, a residue involved in the phosphate transfer reaction. *Mol Cell Biol* [Internet] 1996 [cited 2016 May 30]; 16:1722-33. Available from: <http://mcb.asm.org/content/16/4/1722.abstract>; <http://dx.doi.org/10.1128/MCB.16.4.1722>
- [39] Blommaert EF, Krause U, Schellens JP, Vreeling-Sindelarova H, Meijer AJ. The phosphatidylinositol 3-kinase inhibitors wortmannin and LY294002 inhibit autophagy in isolated rat hepatocytes. *Eur J Biochem* [Internet] 1997 [cited 2016 Jun 7]; 243:240-6. Available from: <http://www.ncbi.nlm.nih.gov/pubmed/9030745>; <http://dx.doi.org/10.1111/j.1432-1033.1997.0240a.x>
- [40] Dall'Armi C, Devereaux KA, Di Paolo G. The role of lipids in the control of autophagy. *Curr Biol* [Internet] 2013 [cited 2016 Jun 7]; 23:R33-45. Available from: <http://www.ncbi.nlm.nih.gov/pubmed/23305670>; <http://dx.doi.org/10.1016/j.cub.2012.10.041>
- [41] Cebollero E, van der Vaart A, Reggiori F. Understanding phosphatidylinositol-3-phosphate dynamics during autophagosome biogenesis. *Autophagy* [Internet] 2012 [cited 2016 Jun 7]; 8:1868-70. Available from: <http://www.ncbi.nlm.nih.gov/pubmed/22992453>; <http://dx.doi.org/10.4161/auto.22162>
- [42] Kotaja N, Lin H, Parvinen M, Sassone-Corsi P. Interplay of PIWI/Argonaute protein MIWI and kinesin KIF17b in chromatoid bodies of male germ cells. *J Cell Sci* 2006; 119:2819-25; PMID:16787948; <http://dx.doi.org/10.1242/jcs.03022>
- [43] Reuter M, Berninger P, Chuma S, Shah H, Hosokawa M, Funaya C, Antony C, Sachidanandam R, Pillai RS. Miwi catalysis is required for piRNA amplification-independent LINE1 transposon silencing. *Nature* 2011; 480:264-7; PMID:22121019; <http://dx.doi.org/10.1038/nature10672>
- [44] Vasileva A, Tiedau D, Firooznia A, Müller-Reichert T, Jessberger R. Tdrd6 is required for spermiogenesis, chromatoid body architecture, and regulation of miRNA expression. *Curr Biol* 2009; 19:630-9; PMID:19345099; <http://dx.doi.org/10.1016/j.cub.2009.02.047>
- [45] Axe EL, Walker SA, Manifava M, Chandra P, Roderick HL, Habermann A, Griffiths G, Ktistakis NT. Autophagosome formation from membrane compartments enriched in phosphatidylinositol 3-phosphate and dynamically connected to the endoplasmic reticulum. *J Cell Biol* [Internet] 2008 [cited 2016 Jun 16]; 182:685-701. Available from: <http://www.ncbi.nlm.nih.gov/pubmed/18725538>; <http://dx.doi.org/10.1083/jcb.200803137>
- [46] Ylä-Anttila V, Vihinen H, Jokitalo E, Eskelinen E-L. Monitoring autophagy by electron microscopy in mammalian cells. *Methods Enzymol* [Internet] 2009 [cited 2016 Jun 16]; 452:143-64. Available from: <http://www.ncbi.nlm.nih.gov/pubmed/19200881>
- [47] Haraguchi CM, Mabuchi T, Hirata S, Shoda T, Hoshi K, Akasaki K, Yokota S. Chromatoid bodies: aggresome-like characteristics and degradation sites for organelles of spermiogenic cells. *J Histochem Cytochem* 2005; 53:455-65; PMID:15805420; <http://dx.doi.org/10.1369/jhc.4A6520.2005>
- [48] Parvinen M. The chromatoid body in spermatogenesis. *Int J Androl* 2005; 28:189-201; PMID:16048630; <http://dx.doi.org/10.1111/j.1365-2605.2005.00542.x>
- [49] Korolchuk VI, Saiki S, Lichtenberg M, Siddiqi FH, Roberts EA, Imarisio S, Jahreiss L, Sarkar S, Futter M, Menzies FM, et al. Lysosomal positioning coordinates cellular nutrient responses. *Nat Cell Biol* [Internet] 2011 [cited 2015 Aug 6]; 13:453-60. Available from: <http://www.pubmedcentral.nih.gov/articlerender.fcgi?artid=3071334&tool=pmcentrez&rendertype=abstract>; <http://dx.doi.org/10.1038/ncb2204>
- [50] Svenning S, Johansen T. Selective autophagy. *Essays Biochem* [Internet] 2013 [cited 2015 Aug 14]; 55:79-92. Available from: <http://www.ncbi.nlm.nih.gov/pubmed/24070473>; <http://dx.doi.org/10.1042/bse0550079>
- [51] Lippai M, Lów P. The role of the selective adaptor p62 and ubiquitin-like proteins in autophagy. *Biomed Res Int* [Internet] 2014 [cited 2015 Aug 6]; 2014:832704. Available from: <http://www.pubmedcentral.nih.gov/articlerender.fcgi?artid=4075091&tool=pmcentrez&rendertype=abstract>
- [52] Guo H, Chitiprolu M, Gagnon D, Meng L, Perez-Iratxeta C, Lagace D, Gibbins D. Autophagy supports genomic stability by degrading retrotransposon RNA. *Nat Commun* [Internet] 2014 [cited 2015 May 30]; 5:5276. Available from: <http://www.ncbi.nlm.nih.gov/pubmed/25366815>; <http://dx.doi.org/10.1038/ncomms6276>
- [53] Fujii Y, Onohara Y, Fujita H, Yokota S. Argonaute2 Protein in Rat Spermatogenic Cells Is Localized to Nuage Structures and LAMP2-

- Positive Vesicles Surrounding Chromatoid Bodies. *J Histochem Cytochem* [Internet] 2016 [cited 2016 Jun 8]; 64:268-79. Available from: <http://www.ncbi.nlm.nih.gov/pubmed/27029769>; <http://dx.doi.org/10.1369/0022155416638840>
- [54] Eulalio A, Behm-Ansmant I, Schweizer D, Izaurralde E. P-body formation is a consequence, not the cause, of RNA-mediated gene silencing. *Mol Cell Biol* [Internet] 2007 [cited 2016 May 4]; 27:3970-81. Available from: <http://mcb.asm.org/content/27/11/3970>; <http://dx.doi.org/10.1128/MCB.00128-07>
- [55] Belevich I, Joensuu M, Kumar D, Vihinen H, Jokitalo E. Microscopy Image Browser: A platform for segmentation and analysis of multidimensional datasets. *PLoS Biol* 2015; 14:e1002340.in press
- [56] Kankaanpää P, Paavolainen L, Tiitta S, Karjalainen M, Päivärinne J, Nieminen J, Marjomäki V, Heino J, White DJ. BioImageXD: an open, general-purpose and high-throughput image-processing platform. *Nat Methods* 2012; 9:683-9; PMID:22743773; <http://dx.doi.org/10.1038/nmeth.2047>
- [57] Kotaja N, Kimmins S, Brancorsini S, Hentsch D, Vonesch JL, Davidson I, Parvinen M, Sassone-Corsi P. Preparation, isolation and characterization of stage-specific spermatogenic cells for cellular and molecular analysis. *Nat Methods* 2004; 1:249-54; PMID:16144087; <http://dx.doi.org/10.1038/nmeth1204-249>
- [58] Bryant JM, Meyer-Ficca ML, Dang VM, Berger SL, Meyer RG. Separation of spermatogenic cell types using STA-PUT velocity sedimentation. *J Vis Exp* 2013; 80: e50648; PMID:24145866
- [59] Robinson MD, McCarthy DJ, Smyth GK. edgeR: a Bioconductor package for differential expression analysis of digital gene expression data. *Bioinformatics* 2010; 26:139-40; PMID:19910308; <http://dx.doi.org/10.1093/bioinformatics/btp616>
- [60] Li XZ, Roy CK, Dong X, Bolcun-Filas E, Wang J, Han BW, Xu J, Moore MJ, Schimenti JC, Weng Z, et al. An ancient transcription factor initiates the burst of piRNA production during early meiosis in mouse testes. *Mol Cell* [Internet] 2013 [cited 2014 Jan 24]; 50:67-81. Available from: <http://www.pubmedcentral.nih.gov/articlerender.fcgi?artid=3671569&tool=pmcentrez&rendertype=abstract>; <http://dx.doi.org/10.1016/j.molcel.2013.02.016>
- [61] Han BW, Wang W, Zamore PD, Weng Z. piPipes: a set of pipelines for piRNA and transposon analysis via small RNA-seq, RNA-seq, degradome- and CAGE-seq, ChIP-seq and genomic DNA sequencing. *Bioinformatics* 2015; 31:593-5; PMID:25342065; <http://dx.doi.org/10.1093/bioinformatics/btu647>
- [62] Trapnell C, Hendrickson DG, Sauvageau M, Goff L, Rinn JL, Pachter L. Differential analysis of gene regulation at transcript resolution with RNA-seq. *Nat Biotechnol* 2013; 31:46-53; PMID:23222703; <http://dx.doi.org/10.1038/nbt.2450>
- [63] Korhonen HM, Meikar O, Yadav RP, Papaioannou MD, Romero Y, Da Ros M, Herrera PL, Toppari J, Nef S, Kotaja N, et al. Dicer is required for haploid male germ cell differentiation in mice. *PLoS One* 2011; 6:e24821; PMID:21949761; <http://dx.doi.org/10.1371/journal.pone.0024821>